Study of characteristics of triple GEM detector for CBM experiment

Project report submitted for the degree of Master of Science

By

Sayak Chatterjee

Roll No. BICU/PSc/2016-18/06

Supervisor

Dr. Saikat Biswas

Bose Institute, Department of Physics

2018

Acknowledgments

First, I would like to thank Dr. Saikat Biswas, for his constant support and encouragement in my project and the writing of this report. I sincerely grateful for his guidance and support during the period of this work and most of all, his patience and understanding.

I would like to thank to Dr. Rajarsi Ray for his help, interesting discussions and patience during the entire M.Sc. course.

I would also like to thank Dr. Supriya Das and Dr. Sidharth K. Prasad for their valuable suggestion and lectures that helped me a lot to complete my report.

I would like to thank Prof. Sanjay K. Ghosh and Prof. Sibaji Raha, for their valuable suggestions and discussions during the course of the study.

I would also like to thank my senior Ms. Shreya Roy for helping me in all possible ways to analyze the results of my experiments and to understand the basic physics of the detectors.

I would like to thank all of my classmates for their valuable comments and suggestions during the entire duration of the project.

I would like to thank all the Bose Institute staff's and specially Mr. Sourav Roy for helping me to make different things which I have used in my experimental setup.

Last but not the least I would like to thank my parents for their patience and constant support.

Abstract of The Report

Gas Electron Multiplier (GEM) detectors have widely been used as tracking devices in particle and heavy-ion physics experiments because of their good efficiency, high rate capability, fast timing, good position resolution features. Triple GEM chambers will be used for tracking purpose in the Muon Chamber (MUCH) of Compressed Baryonic Matter (CBM) experiment at the Facility of Antiproton and Ion Research (FAIR). This brings the strict necessity to know the characteristics of the detectors, its stability and also the uniformity of the response over its active area. A systematic study of the characteristics of a prototype triple GEM detector has been carried out in terms of its variation of gain, energy resolution and efficiency with voltage. Long-term stability and uniformity of the GEM detector has been studied over the active surface area of the prototype GEM detector having dimension 10 cm$\times$10 cm. These experiments has been carried out with Argon, CO_2 gas mixtures in different ratios using Fe^{55} X-ray source, a low noise charge sensitive preamplifier and conventional NIM electronics. Detailed of the test setup and results are presented in this report.

Contents

1 Introduction **9**
- 1.1 History of Detectors: . . . 9
- 1.2 Classification of Detectors: . . . 11
  - 1.2.1 Gaseous Ionization Detectors: . . . 11
  - 1.2.2 Scintillation Detectors: . . . 11
  - 1.2.3 Semiconductor Detectors: . . . 12
- 1.3 Project Objective/Aim: . . . 12

2 Gaseous Detectors **13**
- 2.1 General Principle: . . . 13
- 2.2 Ionization: . . . 17
  - 2.2.1 Energy Loss: . . . 17
  - 2.2.2 Primary and Total Ionization: . . . 18
  - 2.2.3 Collisions: . . . 19
- 2.3 Transport of Electrons and Ions in Gases: . . . 20
  - 2.3.1 Diffusion: . . . 20
  - 2.3.2 Drift and Mobility: . . . 22
- 2.4 Amplification: . . . 23
- 2.5 Gas Mixture: . . . 25

3 Electronic Modules **26**
- 3.1 Introduction: . . . 26
- 3.2 NIM bin: . . . 27
- 3.3 Basic Modules . . . 28
  - 3.3.1 High Voltage Module: . . . 28
  - 3.3.2 Preamplifier: . . . 28
  - 3.3.3 Linear Fan In - Fan Out (FIFO): . . . 29
  - 3.3.4 Discriminator: . . . 29
  - 3.3.5 Single channel Analyzers: . . . 30

3.3.6 Multichannel Analyzers: 31
3.3.7 Digital Storage Oscilloscope: 31
3.3.8 Scaler / Counter : 32
3.4 Discussion about logic signals 32

4 Basic characterization of GEM detector 34
4.1 Introduction: 34
4.2 The GEM detector: 35
4.2.1 GEM Foil: 35
4.2.2 Working principle of GEM detector: 37
4.3 Detector descriptions and experimental setup 39
4.4 Result 40

5 Uniformity Study 46
5.1 Results of the Uniformity Study 46
5.2 Discussions 50

6 Study of Stability 51
6.1 Results of the stability study 51
6.2 Discussions 62

7 Summary and Future Plans 63
7.1 Summary 63
7.2 Future Plans 64

List of Figures

2.1 Basic construction of a simple gas ionization detector 14
2.2 Number of ions collected versus applied voltage in a single wire gas chamber 15
2.3 Average energy loss per unit length as a function of the momentum of various particles in liquid hydrogen, helium gas, carbon, aluminum, iron, tin and lead . . 18

3.1 Pin assignments for NIM standard connector between bin and module 27
3.2 CAEN 4 channel HV programmable power supply module N1470 28
3.3 CAEN Quad linear FAN IN - FAN OUT module N625 29
3.4 CAEN 8 CH LED module N840 30
3.5 Ortec 590A AMP & TSCA module 30
3.6 CAEN module N1145 Quad scaler 32
3.7 NIM logic standards 32

4.1 Double-Masking (left) & Single-Masking (right) GEM foil manufacturing process 36
4.2 Specification of the GEM foil (Left) &; electric field lines in the GEM holes (right) 36
4.3 Voltage divider network of the triple GEM detector . 37
4.4 Working principle of triple GEM detector 38
4.5 Voltage divider network of the triple GEM detector . 39
4.6 Schematic representation of the electronics setup. . . 40
4.7 Count rate as a function of the GEM voltage. 41
4.8 Energy spectra of the GEM detector at different GEM voltage 42
4.9 The gain and the energy resolution as a function of the GEM voltage. 43

4.10 Count rate as a function of the GEM voltage 44
4.11 Energy spectra of the GEM detector at different GEM voltage (up) and the gain and the energy resolution as a function of the GEM voltage (down). 45

5.1 Uniformity in gain over the central active area of the detector 47
5.2 Uniformity in energy resolution over the central active area of the detector 47
5.3 Uniformity in count rate over the central active area of the detector 48
5.4 Distribution of gain over the active region of the detector 48
5.5 Distribution of energy resolution over the active region of the detector 49
5.6 Distribution of count rate over the active region of the detector 50

6.1 Variation of the measured gain and T/p as a function of the time. 52
6.2 Correlation plot: Variation of the gain as a function of T/p. 53
6.3 Variation of the normalised gain as a function of the charge per unit area i.e. dq/dA. 53
6.4 The distribution of the normalised gain. 54
6.5 Variation of the energy resolution and T/p as a function of time. 55
6.6 Energy resolution as a function of T/p. 55
6.7 Normalised energy resolution as a function of the charge per unit area. 56
6.8 The distribution of the normalised energy resolution. 57
6.9 Variation of the measured gain and T/p as a function of the time 58
6.10 Correlation plot: Variation of the gain as a function of T/p 58
6.11 Variation of the normalised gain as a function of the charge per unit area 59
6.12 Distribution of normalised gain 59
6.13 Variation of the energy resolution and T/p as a function of time 60

6.14 Correlation plot: Energy resolution as a function of T/p 60
6.15 Normalised energy resolution as a function of charge per unit area 61
6.16 Distribution of the normalised energy resolution . . . 61

Chapter 1

Introduction

1.1 History of Detectors:

Since the discovery of X-rays by Wilhelm Rontgen in the 1895, the development of various kind of radiation detectors began to play a key role in describing and analyzing different properties of radiation and interactions with matter. Initially, the detectors were only capable of counting the number of particles passing through it and measuring particle's energy. Presently the Time Projection Chamber (TPC) detectors are capable of measuring the energy, momentum of a particle determining its trajectory. The evolution of radiation detectors starts with J. J. Thomsons detector just a few months after the initial discovery of the unknown X-rays . During that time design was relatively simple such that an ion chamber had one positive and one negative flat electrode separated by air. The readings from the chamber were obtained by measuring the current across the two electrodes, that provided major discoveries and the fundamentals of radiation interactions with matter. Some of the major findings were that the air, can turn conductive when a radiation particle passes through sensitive volume of the detector, and that by changing the voltage drop across the electrodes changes the number of electrons that are being collected up to a certain point after which the number stays constant.

The observation of John Townsend, that a significant increase in an ion chambers current is produced at reduced gas pressures when the high voltage is increased well beyond that at which the

saturation current is reached, led to the invention of the first counting tubes (today known as proportional counters) by Rutherford and Hans Geiger in 1908. Townsends explanation was that the increased velocity of the electrons traveling to the collecting electrode permitted them to ionize the air or gas molecules. It was this additional ionization that produced pulses large enough to be counted. Shortly after the invention of the proportional counter the voltage across the electrodes have been increased even further what gave a base for the creation of Geiger Mueller tubes with one large pulse in 1928. Even though the possibility of light output from a barium platinocyanide screen when exposed to X-rays has been known since the 1895, it was not until the Manhattan Project that activities contributed to the development of new kind of radiation detector, the scintillator detector, in 1944. Around the same time, Bell Laboratories invented the semiconductor detector that uses the reverse biased p-n junction to detect alpha particles. From these times, independent of the size, shape and purpose of any radiation detector, all detectors can be divided into three main groups. Gas filled detectors, solid state detectors and scintillation detectors. Radiation detectors in general have been continuously improving and developing since these early times by studying the same basic principles that were discovered and used in these first detector prototype.

During more recent years (1968), the invention of the Multi Wire Proportional Counter (MWPC) at CERN stands out in gas detector development. The MWPC provided a breakthrough in particle detection as it is capable of both particle tracking and energy reading. For this reason, the inventor Georges Charpak was awarded the Nobel Prize in Physics in 1992. However, the efficiency and gain of MWPC reduces with increasing rate because of positive ion space charges which dynamically modifying the electric fields. The problem initiated the search for a new device that could multiply the signal (the electrons from primary ionization) prior to the MWPC. In 1988 at the Institute Laue-Langevin (ILL) in Grenoble, Anton Oed developed a new detector concept named micro-strip gas counter (MSGC), which promised to improve the rate capability and also to make the detector more reliable for long runs. But unfortunately this development did not help much because various operating instabilities like time dependent gain shifts, polarization and charging

up of the substrate, permanent deterioration during sustained irradiation had been observed. In 1997 Fabio Sauli introduced a new concept which is called Micro Pattern Gaseous Detectors (MPGD), and the Gas Electron Multiplier (GEM) detector belongs to this group. [1]

1.2 Classification of Detectors:

Detection of radiation is entirely possible due to the interaction of radiation with the matter. As a result of interaction, photons, electron-ion or electron-hole pairs are produced. Depending on the active medium and detection techniques, detectors are broadly classified into three groups, namely Gaseous detectors or Gaseous Ionization detectors, Scintillation detectors and semiconductor detectors.

1.2.1 Gaseous Ionization Detectors:

Gaseous detectors are radiation detection instruments used in particle physics to detect the presence of ionizing particles, and in radiation protection applications to measure ionizing radiation. It usually involves the mechanism of ionization of the gas molecule by the external radiation and detect the electrons produced due to the primary ionization process with the help of suitable electric field strength and electronics.

1.2.2 Scintillation Detectors:

The term Scintillation means minute flashes of light. As the name suggests, this detectors show their response to the external radiations by giving out some photons having certain wavelengths depending on the material used. Using photomultiplier tubes we can detect those photons and then from that information we can get the information about the external radiations.

1.2.3 Semiconductor Detectors:

A semiconductor detector is a device that uses a semiconductor (usually silicon or germanium) to detect external radiations. In these detectors, radiation is measured by means of the number of charge carriers set free in the detector, which is arranged between two electrodes. Ionizing radiation produces free electrons and holes. The number of electron-hole pairs depends on the energy transmitted by the radiation to the semiconductor. As a result, a certain number of electrons are transferred from the valence band to the conduction band, and an equivalent number of holes are created in the valence band. Under the influence of an electric field, electrons as well as holes travel to the electrodes, where they give rise to a pulse that can be measured in an outer circuit to obtain the information about the ionizing radiation.

1.3 Project Objective/Aim:

In the CBM experiment at FAIR, Germany [2], we will explore the QCD phase diagram at moderate baryonic density. In the CBM experiment one of the biggest challenge is to detect J/ψ (charmonium) at a high interaction rate. One of the largest components of CBM experimental setup is the MUon CHamber (MUCH). The muon chamber will use several hadron absorber made of graphite and iron and sophisticated gaseous detectors. Triple GEM detectors will be used in the first two stations of CBM-MUCH. It is found in simulation that the incident particle rate in the 1st station of CBM MUCH will be about 1 MHz/cm^2 and CBM will run for several years. So one of the major requirements is the stable operation of the detectors for long period. We have studied the characteristics and long term stability of a 10 cm$\times$10 cm double mask triple GEM detector prototype using Ar/CO_2 gas mixture.

Main objective of this study is to investigate the long term stability test of the triple GEM detector using Fe^{55} X-ray, and also to study the uniformity of gain, energy resolution and count rate over the central active area using Ar/CO_2 gas mixture in different ratios.

Chapter 2

Gaseous Detectors

In this chapter we are going to discuss the general principle of Gaseous detectors, different regions of operation and also some basic ideas like primary, secondary ionization, transport phenomena for electrons and ions in the gas mixtures, charge multiplication process. [3, 4]

2.1 General Principle:

Ionization detectors or gaseous detectors are the first electrical devices developed for radiation detection. These instruments are based on the direct collection of the electrons and ions produced in a gas by passing radiation. During the first half of the century, three basic types of detector were developed: the ionization chamber, the proportional counter and the Geiger-Muller counter. They are, however, still very much employed in the laboratory as radiation monitors.

The three original gas devices, i.e., the ionization chamber, the proportional counter and the Geiger-Muller counter, serve as a good illustration of the application of gas ionization phenomena in this class of instruments. These detectors are actually the same device working under different operating parameters, exploiting different phenomena. The basic configuration (Figure 2.1) consists of a container, which we will take to be a cylinder for simplicity, with con-

ducting walls and a thin end window. The cylinder is filled with a suitable gas, usually a noble gas such as argon.

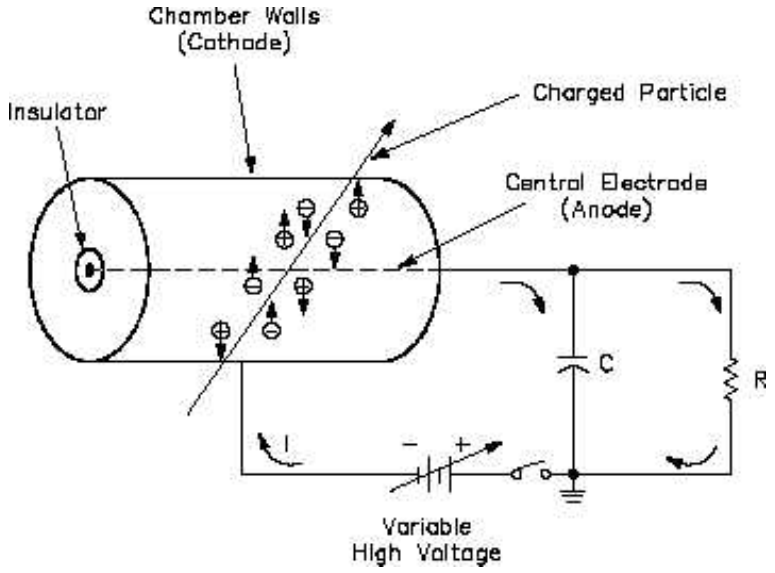

Figure 2.1: Basic construction of a simple gas ionization detector

Along its axis is suspended a conducting wire to which a positive voltage, say +V, relative to the walls is applied. A radial electric field E=$\frac{v}{rln(b/a)}$ with r: radial distance from axis; b: inside radius of cylinder; a: radius of central wire is thereby established. If radiation now penetrates the cylinder, a certain number of electron-ion pairs will be created, either directly, if the radiation is a charged particle, or indirectly through secondary reactions if the radiation is neutral. The mean number of pairs created is proportional to the energy deposited in the counter. Under the action of the electric field, the electrons will be accelerated towards the anode and the ions toward the cathode where they are collected.

The current signal observed, however, depends on the field intensity. This is illustrated in Figure 2.2 which plots the total charge collected as a function of applied voltage.

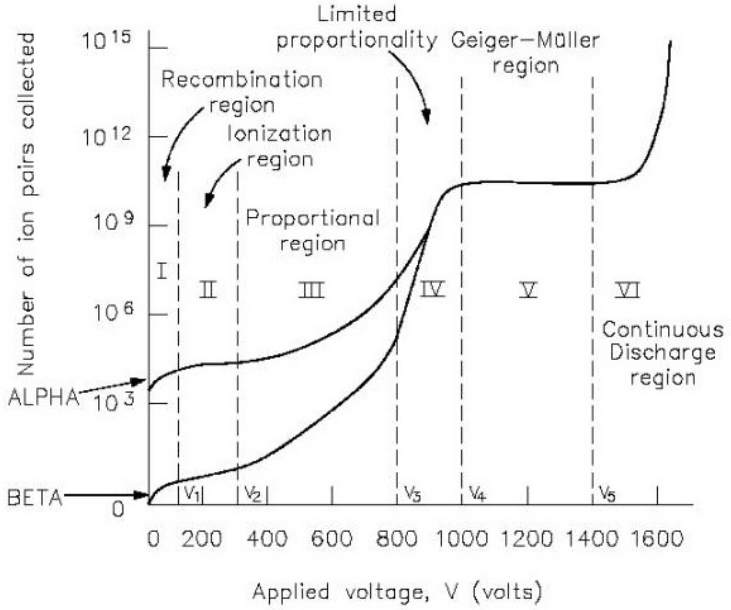

Figure 2.2: Number of ions collected versus applied voltage in a single wire gas chamber

At very low voltage about zero volt, no charge is collected as the ion-electron pairs recombine under their own electrical attraction. This region is known as 'Recombination region'.

As the voltage is increased, the recombination forces are overcome and the current begins to increase and the number of collected electron-ion pair increases. At some point, all created pairs will be collected and further increase in voltage show no effect. This corresponds to the first flat region of the figure 2.2, which is known as 'Ionization region'. Detectors working in this region are called 'Ionization Chamber'.

As the voltage is further increased beyond ionization region, we find from the figure 2.2 that the current increases again with the applied voltage. At this point, the electric field is strong enough to accelerate free electrons to an energy where they are also capable of ionizing gas molecules in the cylinder. The electrons liberated in these secondary ionization then accelerate to produce still more

ionization and so on. This results in an ionization avalanche. Since the electric field is strongest near the anode, as seen from figure 2.1, this avalanche occurs very quickly and almost entirely within a few radii of this wire. The number of electron-ion pairs in the avalanche, however, is directly proportional to the number of primary electrons. What results then is a proportional amplification of the current, with a multiplication factor depending on the working voltage V. That is why this region is called 'Proportional region'. Detectors operating in this domain are known as 'Proportional Chamber'.

If the voltage is now increased beyond proportional region, the total amount of ionization created through multiplication becomes sufficiently large that the space charge created distorts the electric field about the anode. Proportionality thus begins to be lost. This is known as the region of limited proportionality.

Increasing the applied voltage still higher, the energy becomes so large that a discharge occurs in the gas. What happens physically is that instead of a single, localized avalanche at some point along the anode wire, a chain reaction of many avalanches spread out along the entire length of the anode is triggered. These secondary avalanches are caused by photons emitted by deexciting molecules which travel to other parts of the counter to cause further ionizing events. The output current thus becomes completely saturated, always giving the same amplitude regardless of the energy of the initial event. This region is known as 'Geiger-Muller region' and detectors working in this voltage region are called Geiger-Muller or breakdown counter.

Finally, now, if the voltage is increased still further a continuous breakdown occurs with or without radiation. This region, of course, is to be avoided to prevent damage to the detector.

2.2 Ionization:

2.2.1 Energy Loss:

A relativistic charged particle going through a volume of gas, or more generally through matter, will interact with its constituents and by doing so the particle will loose some energy along its trajectory. The particle can interact in several ways. Depending on its type, the particle can interact through weak interaction, strong interaction, or electromagnetic interaction. In the gaseous detector, the dominating interaction is the electromagnetic interaction. There are several electromagnetic interactions possible, But the dominant one in our case is the Coulomb interaction. This interaction will excite and/or ionize gas molecules. The energy loss by unit length of a relativistic charged particle is described by the Bethe-Bloch equation,

$$-\left\langle \frac{dE}{dx} \right\rangle = K z_{in}^2 \frac{Z}{A} \frac{1}{\beta^2} [\frac{1}{2} ln \frac{2 m_e c^2 \beta^2 \gamma^2 T_{max}}{I^2} - \beta^2 - \frac{\delta(\beta\gamma)}{2}] \quad (2.1)$$

Where $\mathrm{K} = 4\pi \mathrm{N}_a \mathrm{r}_e^2 \mathrm{m}_e \mathrm{c}^2$

T_{max} is the maximum kinetic energy given to a free electron during a collision, z_{in} the charge of incident particle, m_e the electron mass, β is the velocity of the particle divided by the speed of light ($\beta = \frac{v}{c}$), γ is the Lorentz factor ($\gamma = (1-\beta^2)^{-1/2}$), I is the mean excitation energy, A and Z are respectively the mass number and the atomic number of the material, N_a the Avogadro number and r_e the classical radius of the electron defined as $\mathrm{r}_e = \frac{e^2}{\pi \varepsilon_0 m_e c^2}$ (e is the electrons charge and ε_0 is the vacuum permettivity).

The Bethe-Bloch function is shown in Figure 2.3 for different materials. We can see that the energy loss does not depend on the mass of the particle, but only on the speed and charge of the particle.

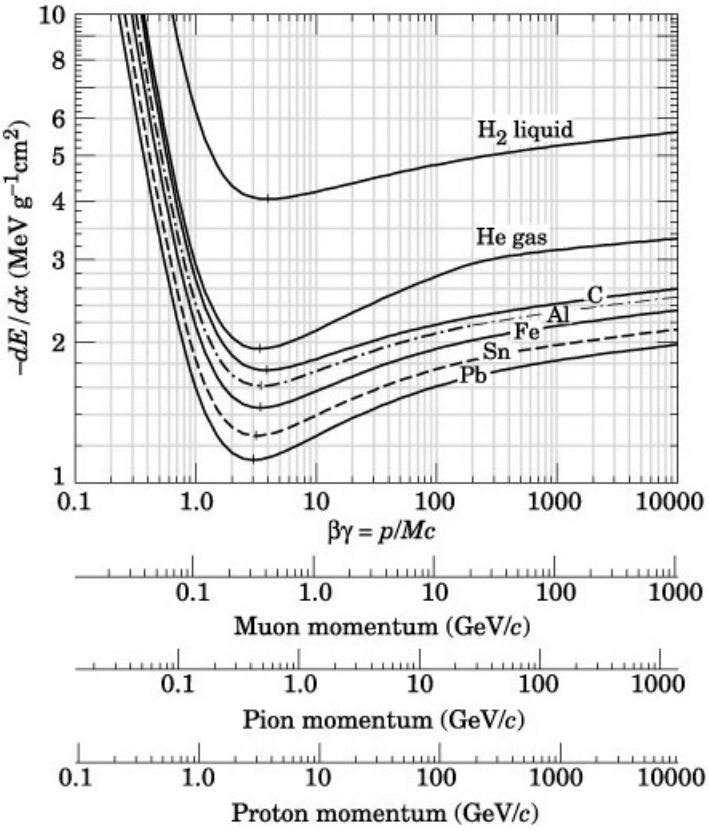

Figure 2.3: Average energy loss per unit length as a function of the momentum of various particles in liquid hydrogen, helium gas, carbon, aluminum, iron, tin and lead

2.2.2 Primary and Total Ionization:

The incoming radiation will create electron-ion pairs along the trajectory by electromagnetic interaction. This mechanism is called primary ionization. If the resulting released electrons have an energy larger than the ionization potential of the medium, they will also ionize other molecules of the gas. This is called secondary ionization. The sum of both primary and secondary ionization's is called total ionization.

If we define W the mean energy loss needed to create a ion-electron pair, we can write a relation giving the average total number of produced pairs along the trajectory $\langle N \rangle$ as,

$$W \langle N \rangle = L \left\langle \frac{dE}{dx} \right\rangle \tag{2.2}$$

Where L is the trajectory length. The energy needed to create a pair depends on the gas mixture and is experimentally determined.

From equation (2.2), we can easily express the average number of pairs created per unit length (n) as,

$$n = \frac{\langle dE/dx \rangle}{W} \tag{2.3}$$

In case of gas mixtures, the total number of electrons is obtained by summing the mean number of produced electrons in every gas of the mixture, weighted by the gas percentage P_i in the mixture. So the number of pairs created in case of gas mixtures can be expressed as,

$$n = \sum_{i=1}^{n} \left\langle \frac{dE}{dx} \right\rangle_i \frac{P_i}{W_i} \tag{2.4}$$

where the index i represents a gas among n gases in the mixture.

2.2.3 Collisions:

When a charged particle crosses a gas volume it collides with a large number of gas molecules, but only a few of these collisions actually produce ionization. The probability distribution that will follow this ionization will therefore be a Poisson distribution. If we have a mean value of n primary electrons over a certain distance, the probability to create k primary electrons is given by,

$$P(k) = \frac{n^k}{k!} e^{-n} \tag{2.5}$$

With this expression, we can compute the probability that the incident particle does not ionize the gas, i.e. the particle can not be detected. Therefore, the minimum inefficiency of a perfect detector is given by,

$$P(k = 0) = e^{-n} \tag{2.6}$$

i.e. the probability that there are no primary ionization when passing through the gas volume.

2.3 Transport of Electrons and Ions in Gases:

For gaseous detectors, an understanding of the motion of the electrons and ions in gases is extremely important as these factors influence many operating characteristics of the detector. For the most part, this motion is described by the classical kinetic theory of gases.

2.3.1 Diffusion:

In the absence of an electric field, electrons and ions liberated by passing radiation diffuse uniformly outward from their point of creation. In the process they suffer multiple collisions with the gas molecules and lose their energy. They thus come quickly into thermal equilibrium with the gas and eventually recombine. At thermal energies, the velocities of the charges are described by the Maxwell distribution which gives a mean speed of

$$v = \sqrt{\frac{8k_B T}{\pi m}} \tag{2.7}$$

where k_B is Boltzmann constant, T the temperature and m the mass of the particle. Quite obviously, the average speed of the electrons is much greater than that of the ions due their smaller mass.

From kinetic theory, the linear distribution of charges after diffusing a time t can be shown to be Gaussian,

$$\frac{dN}{dx} = \frac{N_0}{\sqrt{4\pi Dt}} exp(-\frac{x^2}{4Dt}) \tag{2.8}$$

where N_o is the total number of charges, x the distance from the point of creation and D the diffusion coefficient. The rms spread in x is thus

$$\sigma(x) = \sqrt{2Dt} \tag{2.9}$$

If three dimensions are considered, the spherical spread is given by,

$$\sigma(x) = \sqrt{6Dt} \tag{2.10}$$

where r is the radial distance. The diffusion coefficient is a parameter which can be calculated from kinetic theory and can be shown to be,

$$D = \frac{1}{3} v\lambda \tag{2.11}$$

where λ is the mean free path of the electron or ion in the gas. For a classical ideal gas, the mean free path is related to the temperature T, and the pressure p, by

$$\lambda = \frac{k_B T}{\sqrt{2}\sigma p} \tag{2.12}$$

Where σ is the total cross section for a collision with a gas molecule.

From equations (2.7), (2.10), and (2.11) we get the following expression,

$$D = \frac{2}{3\sqrt{\pi}} \frac{1}{p\sigma} \sqrt{\frac{(k_B T)^3}{m}} \tag{2.13}$$

2.3.2 Drift and Mobility:

In the presence of an electric field, the electrons and ions freed by radiation are accelerated along the field lines towards the anode and cathode respectively. This acceleration is interrupted by collisions with the gas molecules which limit the maximum average velocity which can be attained by the charge along the field direction. The average velocity attained is known as the drift velocity of the charge and is superimposed upon its normal random movement.

In kinetic theory, it is useful to define the mobility of a charge as,

$$\mu = u/E \tag{2.14}$$

where u is the drift velocity and E the electric field strength. For positive ions, the drift velocity is found to depend linearly on the ratio E/p (also known as the reduced electric field), up to relatively high electric fields. At a constant pressure, this implies that the mobility μ is a constant. For a given E, it is also quite clear that μ varies as the inverse of the pressure p.

For ideal gases, in which the moving charges remain in thermal equilibrium, the mobility can be shown to be related to the diffusion constant by,

$$\frac{D}{\mu} = \frac{k_B T}{E} \tag{2.15}$$

This is the result of a classical argument and is known as the Einstein relation.

Unlike positive ions, the mobility for electrons is much greater and is found to be a function of E. The gain in velocity of the

electrons may also affect the diffusion rate if the mean energy of the electrons exceeds thermal energies. The factor kT in equation (2.15) is then replaced by this mean energy. The diffusion constant D then increases accordingly causing a greater spread of the electron cloud as given by equations (2.9) and (2.10). This has important consequences for detectors such as the drift chambers which attempt to determine the position of a track by measuring the drift time of the ionization electrons.

2.4 Amplification:

When an electron moves in the gas with enough energy, it may cause ionizing collisions. Consequently, if the electric field exceeds a few kV/cm, electrons can gain sufficient energy between collisions to produce excitation or ionization of the gas molecules, creating additional electron-ion pairs. The produced electrons will in turn be accelerated and therefore be able to further ionize the gas. This multiplication process is called the avalanche. We can define the free mean path of ionization of the electrons, i.e. the average distance an electron must travel before undergoing an ionizing collision with a gas molecule. This distance will depend on the effective ionization cross section $\sigma(\epsilon)$, which itself depends on the energy ϵ it takes to create a pair. The distance also depends on the density of the number of molecules in the gas, say n. This leads to the following expression for the mean free path of ionization,

$$\lambda(\epsilon) = \frac{1}{n\sigma(\epsilon)} \tag{2.16}$$

The inverse of this distance represents the number of electron-ion pairs produced per unit length. This number is called the Townsend coefficient ($\alpha(\epsilon) = \frac{1}{\lambda(\epsilon)}$).

In the case of a constant electric field, an electron will ionize a gas molecule after an average travel of α^{-1} , there is therefore, at that time, two electrons and one ion. The two electrons, after a mean path again equal to α^{-1} , will ionize two gas molecules (on average). And the process will repeat. On a distance dx we have

an increased number of electrons equal to n times the coefficient of Townsend,

$$\frac{dn}{dx} = n\alpha \tag{2.17}$$

Integrating the above expression we get,

$$n = n_0 e^{\alpha x} \tag{2.18}$$

where n_0 is the number of electrons at the start of the avalanche.

So the gain can be defined as,

$$G(\Delta x) = \frac{n}{n_0} = e^{\alpha \Delta x} \tag{2.19}$$

which describes the multiplication factor of the avalanche.

The avalanche, which is a set of electrons and ions, will take the form of a drop. Indeed the difference in drift velocity between electron and ion (which is of the order of 10^3) will result in an accumulation of electrons at the front of the avalanche, while the ions will be distributed all along the avalanche forming a tail. A priory, given the description of the gain, nothing limits the multiplication. However there is of course a limit to the gain. Indeed, the size of the avalanche will increase with the distance. The electric field produced by the space charge will therefore also grow to locally cancel the external electric field. This effect will result in electron/ions recombination which will emit ultraviolet photons in an isotropic direction in the detector. These photons can also ionize the gas molecules which will create new avalanches. All these avalanches can be combined with each other and connect the electrodes by a conducting plasma, which will produce a discharge, which may damage the electrodes. An empirical limit of maximum number of charges in an avalanche was determined by Raether and correspond to,

$$\alpha s \sim 20 \tag{2.20}$$

where s is the characteristic dimension of the avalanche. This limit corresponds to a gain of the order of 10^8 .

2.5 Gas Mixture:

The choice of the gas mixture that we use in a gaseous detector is something quite complicated and depends on the expected performance of the chamber. The important parameters to be taken into account in the choice of the gas mixture for the application studied in this report are, the gain, the ability to absorb ultraviolet photons, which minimizes the discharge, (i.e to maintain the appropriate proportion of the quenchers) and the stability of the detector. The choice of argon is quite conventional, because the primary ionization for minimum ionizing particles is high enough, and compared to other noble gas (like Xenon and Krypton), argon is inexpensive. It happens frequently that we should operate at a high gain, i.e. with a high electric field, which increases the risk of discharges. To increase the electric field while avoiding discharges, a poly-atomic gas is usually added. Indeed, poly-atomic gases have the property of having other degrees of freedom such as rotation, vibration etc. They can therefore absorb ultraviolet photons produced in the avalanche, and thus avoid the discharges. This type of gas is called a quencher. Gases generally used as quenchers are CO_2 , CH_4 etc.

Chapter 3

Electronic Modules

3.1 Introduction:

In this we will discuss about the electronics module used to extract information from the radiation detectors. The two most common nuclear instrumentation standard are, NIM and CAMAC. [3, 4, 5]

The Nuclear Instrumentation Module (NIM) standard defines mechanical and electrical specifications for electronics modules used in experimental particle and nuclear physics. The concept of modules in electronic systems offers enormous advantages in flexibility, interchange of instruments, reduced design effort, ease in updating and maintaining the instruments. It provides a common footprint for electronic modules (amplifiers, ADCs, DACs, discriminators, etc.), which plug into a larger chassis (NIM crate, or NIM bin). The crate must supply 12 and 24 volts DC power to the modules via a back plane, the standard also specifies 6 V DC and 220 V or 110 V AC pins, but not all NIM bins provide them. Mechanically, NIM modules must have a minimum standard width of 1.35 in (34 mm), a maximum face plate height of 8.7 in (221 mm) and depth of 9.7 in (246 mm).

However NIM modules cannot communicate with each other through the crate back plane; this is a feature of later standards such as CAMAC.

Computer-Aided Measurement And Control (CAMAC) is a standard bus which allows data exchange between plug-in modules (up to 24 in a single crate) and a crate controller, which then interfaces to a PC or to a VME-CAMAC interface.

In case of my study, I have used the conventional NIM module.

3.2 NIM bin:

The NIM Bin is designed to fit into the standard 19 inch relay rack and is subdivided into 12 individual module positions across its width.

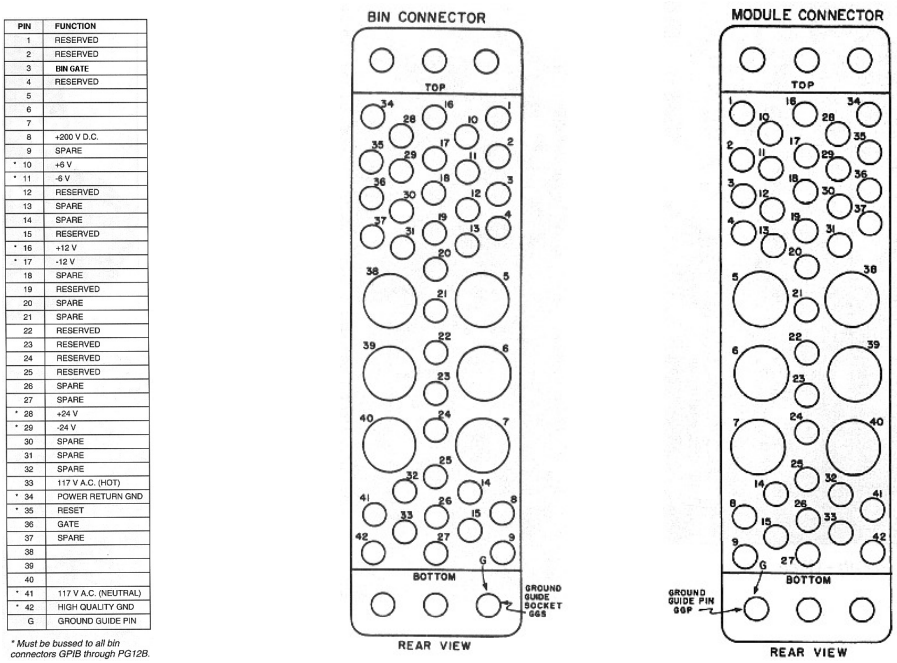

PIN	FUNCTION
1	RESERVED
2	RESERVED
3	BIN GATE
4	RESERVED
5	
6	
7	
8	+200 V D.C.
9	SPARE
* 10	+6 V
* 11	-6 V
12	RESERVED
13	SPARE
14	SPARE
15	RESERVED
* 16	+12 V
* 17	-12 V
18	SPARE
19	RESERVED
20	SPARE
21	SPARE
22	RESERVED
23	RESERVED
24	RESERVED
25	RESERVED
26	SPARE
27	SPARE
* 28	+24 V
* 29	-24 V
30	SPARE
31	SPARE
32	SPARE
33	117 V A.C. (HOT)
* 34	POWER RETURN GND
* 35	RESET
36	GATE
37	SPARE
38	
39	
40	
* 41	117 V A.C. (NEUTRAL)
* 42	HIGH QUALITY GND
G	GROUND GUIDE PIN

* Must be bussed to all bin connectors GPIB through PG12B.

Figure 3.1: Pin assignments for NIM standard connector between bin and module

A NIM module occupies a unit width of 34.4 mm, although integral multiples of this width are permitted corresponding to modules of double width, triple width, and so on. Each of the 12 bin locations

is provided with a 42-pin connector that mates with a corresponding connector at the back of each module. Pin assignments and functions are illustrated in Figure 3.1. Primary dc supply voltages provided by the bin are 12V and 24V. The concept of modules in electronic systems offers enormous advantages in flexibility, interchange of instruments, reduced design effort, ease in updating and maintaining the instruments.

3.3 Basic Modules

3.3.1 High Voltage Module:

High voltage power supply is very important for any detector laboratory.

Regulated high voltage power supply is used to bias any kind of detector. Sometimes multichannel power supply is necessary for a single detector. It basically consists of a step-up transformer that generates the required high voltage. Different detectors require different biasing voltages in the range of a few hundred volts to a few kV. Any desired voltage can be set in the module. The ramp up and ramp down voltages can also be set.

Figure 3.2: CAEN 4 channel HV programmable power supply module N1470

For the stability and uniformity study of triple GEM detector, CAEN 4 channel HV programmable power supply module N1470 has been used. It can supply voltages ranging from 0-8000 Volts.

3.3.2 Preamplifier:

The primary function of a preamplifier is to extract the signal from the detector without significantly degrading the intrinsic signal-to noise ratio, and also to match the impedance between its input and output circuitry. The preamplifier is not designed to give high gain and usually its gain is of the order of 1-10, to amplify

weak signals from a detector and to drive it through the cable that connects the preamplifier with the rest of the equipment. Since the input signal at the preamplifier is generally weak, preamplifiers are normally mounted as close as possible to the detector so as to minimize cable length. Three basic types of preamplifier exist,

1) voltage sensitive,

2) current sensitive,

3) charge sensitive. For GEM detector VV50-2 preamplifier is used.

3.3.3 Linear Fan In - Fan Out (FIFO):

Fan-outs are active circuits which allow the distribution of one signal to several parts of an electronics system by dividing the input signal into several identical signals.

Figure 3.3: CAEN Quad linear FAN IN - FAN OUT module N625

The fan-in, on the other hand, accepts several input signals and delivers the algebraic sum at the output. These modules may be bipolar, i.e., accepting signals of both polarities, or of single polarity. Both fan-ins and fan-outs come in two varieties: linear and logic. The linear modules accept both analog and logic signals, whereas logic fan-outs and fan-ins are designed for logic signals only. In the case of a logic fan-in, the algebraic sum is replaced by a logical sum (i.e., OR). In our laboratory CAEN Quad linear Fan In - Fan Out module N625 is used.

3.3.4 Discriminator:

The discriminator is a device which responds only to input signals with a pulse height greater than a certain threshold value. If

this criterion is satisfied, the discriminator responds by issuing a standard logic signal; if not, no response is made.

The value of the threshold can usually be adjusted manually. The most common use of the discriminator is for blocking out low amplitude noise pulses from detectors. Good pulses, which should in principle be large enough to trigger the discriminator are then transformed into logic pulses for further processing by the following electronics. In this role, the discriminator is essentially a simple analog-to-digital converter. An important aspect of the discriminator is the method of triggering. Because of its use in timing, it is important that the time relation between the arrival of the input pulse and the issuance of the output pulse be constant. In most discriminators, triggering occurs the moment the pulse crosses the threshold level. This is known as leading edge (LE) triggering. For the study on GEM detector CAEN 8 CH LED module N840 has been used.

Figure 3.4: CAEN 8 CH LED module N840

3.3.5 Single channel Analyzers:

The single channel analyzer (SCA) is a device which sorts incoming analog signals according to their amplitudes. Like the discriminator, it contains a lower level threshold below which signals are blocked. In addition, however, there is also an upper level threshold above which signals are rejected. Thus only signals which fall between these two levels provoke a response from the SCA, i.e., a standard logic signal. The opening between the upper and lower level is usu-

Figure 3.5: Ortec 590A AMP & TSCA module

ally called the window. The SCA generally has three working modes:

1) Normal Mode or Differential Mode - In this mode, the upper and lower levels can be adjusted independently of each other.

2) Window Mode - In this mode one sets the lower level and the window width, that is the distance between lower and upper levels.

3) Integral Mode - Here, the upper level is completely removed from the SCA circuit altogether so that one simply has a discriminator with an adjustable lower level.

In this study Ortec 590A AMP & TSCA module is used.

3.3.6 Multichannel Analyzers:

Multichannel analyzers (MCA) are sophisticated devices which sort out incoming pulses according to pulse height and keep count of the number at each height in a multichannel memory. The contents of each channel can then be displayed on a screen or printed out to give a pulse height spectrum. The MCA works by digitizing the amplitude of the incoming pulse with an analog-to-digital converter (ADC). The MCA then takes this number and increments a memory channel whose address is proportional to the digitized value. In this way incoming pulses are sorted out according to pulse height and the number at each pulse height stored in memory locations corresponding to these amplitudes.

3.3.7 Digital Storage Oscilloscope:

To visualize the signal produced by the detector and study various characteristics of the pulse, such as rise time, fall time, pulse height, pulse shape, etc. Digital Storage oscilloscope (DSO) is used. In the DSO one can set trigger and threshold to encounter only useful events and to cutoff the noise respectively. The DSO used in this experiment is from Agilent Technologies, model number DSO6054A and can support up to four different input signal ports.

3.3.8 Scaler / Counter :

The scaler is a unit which counts the number of pulses fed into its input and presents this information on a visual display.

In general, scalers require a properly shaped signal in order to function correctly, thus it is usually necessary to have a discriminator or a pulse shaper process signals from the detector before they can be counted by the scaler. Most commercial scalers are also available with a variety of auxiliary functions such as a gate, preset count, reset, etc. Scaler can accept NIM or TTL signals as input. In this study CAEN module N1145 Quad scaler and preset counter timer is used.

Figure 3.6: CAEN module N1145 Quad scaler

3.4 Discussion about logic signals

NIM modules include both analog and digital instruments. It should be recalled that in analog signals, information is carried in the amplitude or shape of the signal, thus they are of continuously varying heights and form.

Digital or logic signals, on the other hand, are of fixed shape and have only two possible states: yes or no. It is customary to refer to the two states as logical 0 and logical 1, which signal is chosen as 1 or 0 is arbitrary however. Two types of standards exist: slow-positive logic and fast-negative logic. The first refers to signals of relatively slow rise time, on the order of hundreds of nanoseconds or more. They are of positive

Fast Negative NIM

	O/P must deliver	I/P must accept
Logic 1 (high)	-14 mA to -18 mA	-12 mA to -36 mA
Logic 0 (low)	-1 mA to +1 mA	-4 mA to +20 mA

Slow Positive NIM

	O/P must deliver	I/P must accept
Logic 1 (high)	+4 V to +12 V	+3 V to +12 V
Logic 0 (low)	+1 V to -2 V	+1.5 V to -2 V

TTL and ECL Logic

	TTL	ECL
Logic 1 (high)	2 – 5 V	- 1.75 V
Logic 0 (low)	0 – 0.8 V	-0.90 V

Figure 3.7: NIM logic standards

polarity and are used with slow detector systems. While not part of the NIM standard two other logic families are often found in nuclear and particle physics electronics. The first is the TTL (Transistor-Transistor Logic) logic family. This is a positive going logic which is very often found on NIM electronics modules. The second is a logic family which is becoming increasingly popular in high-energy physics. This is the emitter-coupled logic (ECL) family which is currently the fastest form of digital logic available. Figure 3.7 defines the voltage levels for the logic systems described above. Note that the definition is in terms of a voltage across a 1000Ω impedance. This implies that the current carried by the signal is very small. The consequence of this is that slow-positive signals cannot be transmitted through long cables. The characteristic impedance of most cables is not more than about 100Ω . After a meter or two of cable, therefore, the signal becomes highly attenuated. Fast-negative logic, often referred to as NIM logic, employs extremely fast signals with rise times on the order of 1 ns and comparable widths. This type is often used in experiments where high count rates or fast timing is desired.

Chapter 4

Basic characterization of GEM detector

4.1 Introduction:

A major revolution in the area of gaseous detectors occurred in 1968 when Georges Charpak invented the Multiwire Proportional Chamber (MWPC), a gaseous detector outperforming by orders of magnitude the rate capability of contemporary devices. Consisting of a grid of thin, parallel anode wires between two cathode planes, on application of suitable voltages the device collects and amplifies, by avalanche multiplication, the tiny ionization clusters released in a gas by ionizing radiation, permitting detection with electronics means.

Despite their successful use in particle physics experiments and other fields, MWPCs have several limitations. The creation in the multiplication process of large amounts of positive ions, slowly receding towards the cathodes, causes a modification of the applied electric field, and results in a drop of gain at particle fluxes above $\sim 10^4$ mm^{-2}. The discrete wire spacing is itself a limitation to the multi-track resolution, essential at high particle rates and multiplicities. Even more detrimental, the creation and deposit on the anode wires of thin insulating layers caused by the polymerization of organic gases or pollutants may result in an amazingly short operating

life span.

The Micro-Strip Gas Counter (MSGC), introduced by Anton Oed in 1988, seemed to overcome some of the above mentioned limitations. Consisting of a set of thin parallel metallic strips laid on an insulating substrate, alternatively connected as anodes and cathodes, MSGC's provide rate capabilities two orders of magnitude higher than MWPC's, and a tenfold improvement in the multi-track resolution.

Disappointingly, and despite the efforts by many groups, the device appeared to be rather susceptible to irreversible degradation due to occasional but destructive discharges.

The problems met with the MSGC's resulted in a large effort devoted to the development of sturdier structures, preserving its rate and multi-track capabilities. Collectively named Micro-Pattern Gas Detectors (MPGD). Gas Electron Multiplier detector is a variant of MPGD. [6]

4.2 The GEM detector:

The Gas Electron Multiplier detector is a micro pattern gas detector. The main component of this detector is the GEM foil.

4.2.1 GEM Foil:

The GEM foil consists of a kapton foil of 50 μm thick with 5 μm copper cladding surfaces on both sides. Those foils are pierced with a high density of micro-holes (50 to 100 holes per cm^2). The most common technique used to produce those holes is the photo-lithography. Two different techniques of photo-lithography exist to produce GEM foils: Double-Mask and Single-Mask. The Figure 4.1 shows the schematic comparison of both the procedures. By applying a potential difference of a few hundred volts between the two planes of copper, produces an electric field of the order of a few tens of kV/cm in the center of the holes. Figure 4.2 (left)

shows a GEM foil produced by Double-Mask technique and (right) its dimensions and the electric field lines in the neighborhood of the holes .

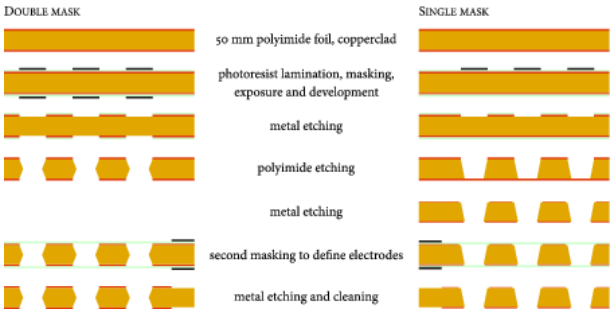

Figure 4.1: Double-Masking (left) & Single-Masking (right) GEM foil manufacturing process

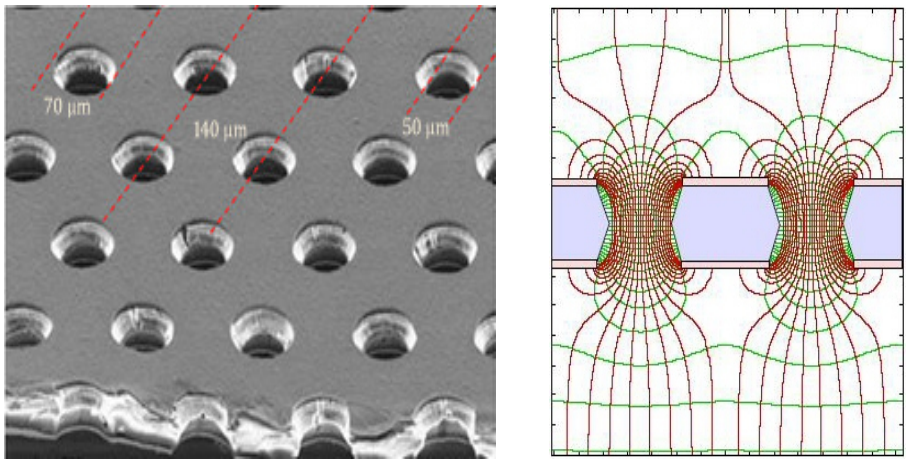

Figure 4.2: Specification of the GEM foil (Left) &; electric field lines in the GEM holes (right)

4.2.2 Working principle of GEM detector:

In this work a GEM detector prototype has been used, consists of three 10 cm $\times$ 10 cm double mask GEM foils. In a typical triple GEM detector the top most electrode is called the drift plane. After that with proper gaps three GEM foils are used & the signals are collected from the readout pad. The gap between the drift plane and the top of the 1^{st} GEM foil is called the drift gap.

The gap between the bottom of the 1^{st} GEM foil and top of the 2^{nd} GEM foil and the gap between bottom of 2^{nd} GEM foil and the top of 3^{rd} GEM foil are called transfer gap 1 and transfer gap 2 respectively. The gap between the bottom the 3^{rd} GEM foil and the readout plane is called the induction gap. The electric field in the drift gap and induction gap are called drift field and induction field respectively. In the present work the drift gap, transfer gap 1, transfer gap 2, induction gap are kept 3 mm, 2 mm, 2 mm, 2 mm respectively. Figure 4.3 shows the basic structure of a triple GEM detector. When any radiation or charged particle enters into the drift region, they first interact with the gas molecules and produce electron-ion pairs. Those electrons are known as primary electrons. Due to the presence of the electric field between the electrode and top of the first GEM foil, the primary electrons are accelerated towards the first GEM foil.

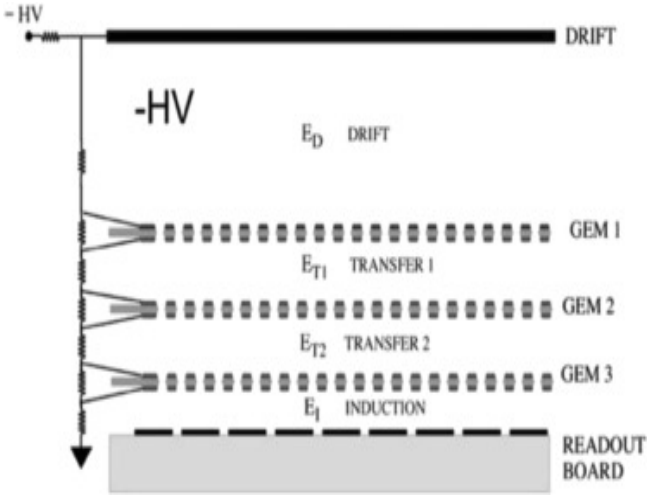

Figure 4.3: Voltage divider network of the triple GEM detector

Due to the geometry of the GEM foils, strength of the electric field becomes very high within the holes, and as a result, the primary electrons gain enough kinetic energy to produce avalanche

multiplication by ionizing the gas molecules there. Thus after the first GEM foil we get large number of electrons. Those electrons are again guided by the field in the transfer gap 1 to the 2^{nd} GEM foil and the same multiplication phenomena occurs for both the 2^{nd} and the 3^{rd} GEM foils and finally the electrons after the 3^{rd} GEM foil is guided to the read out plane by the electric field in the induction gap.

Each of the GEM hole works as an individual proportional counter. During drift and gas amplification, the electrons are subject to diffusion, which causes a fractional amount to be lost to the GEM-electrodes or the Kapton walls.

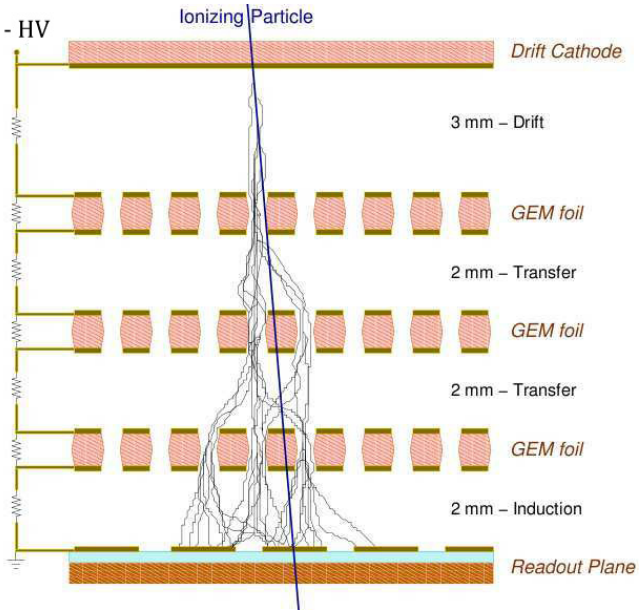

Figure 4.4: Working principle of triple GEM detector

A field dependent fraction of the electron charge is thus collected by the bottom of the GEM electrode, whereas the ions are collected on the top of the electrode. Figure 4.4 shows schematically how the amplification takes place.

The ratio between the number of electrons leaving and entering an amplification stage is called the real gain. Because of the losses occurring at the GEM surfaces, this real gain is not equal to the effective gain which is determined by signal, produced by the induce charges on the readout plane. To increase the gain of the detector without discharge GEM foils can be used in cascaded mode i.e increasing the number of GEM foils and reducing individual ΔV across a single foil. All the electrons produced due to primary ionization are not transferred through the GEM foils, and the fraction

of ionization electrons transferred through the GEM foil is known as transparency of the GEM foil. Transparency depends on the drift fields because depending on the strength of the drift field the field lines go through the holes or terminate on the copper layer. Also due to the diffusion losses inside the holes and the statistical process of the gas amplification, a deflection of the electron trajectory occurs. They will not follow their ideal way through the holes, but some of them will end up at the surfaces. The GEM voltage also plays an important role in the transparency.

4.3 Detector descriptions and experimental setup

In this study, a GEM detector prototype, consisting of three 10 cm $\times$ 10 cm double mask foils, obtained from CERN has been used. The drift, transfer and induction gaps of the detector are kept 3 mm, 2 mm and 2 mm respectively. The high voltages (HV) to the drift plane and individual GEM planes have been applied through a voltage dividing resistor chain as shown in the Figure 4.5.

Although there is a segmented readout pads of size 9 mm $\times$ 9 mm each, the signal in this study was obtained from all the pads added by a sum up board and a single input is fed to a charge sensitive preamplifier (VV50-2).

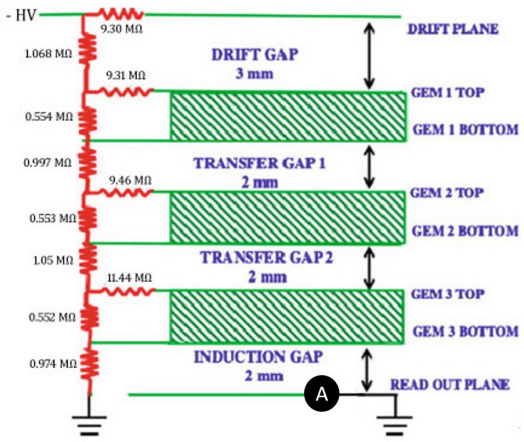

Figure 4.5: Voltage divider network of the triple GEM detector

The gain of the preamplifier is 2 mV/fC with a shaping time of 300 ns. A NIM based data acquisition system is used after the preamplifier. Same signal from the preamplifier is used to measure the rate and to obtain the energy spectrum.

The output signal from the preamplifier is fed to a linear Fan-In-Fan-out (linear FIFO) module for this purpose. The analog signal from the linear FIFO is put to a Single Channel Analyzer (SCA) to measure the rate of the incident particle.

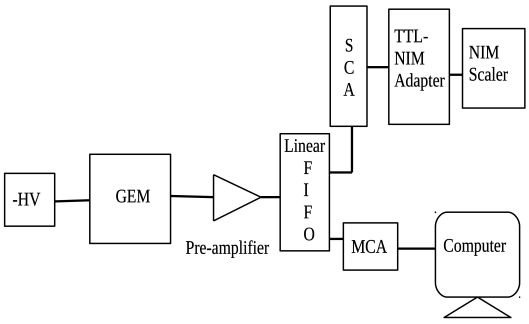

Figure 4.6: Schematic representation of the electronics setup.

The SCA is operated in integral mode and the lower level in the SCA is used as the threshold to the signal. The threshold is set at 0.1 V to reject the noise. The discriminated signal from the SCA, which is TTL in nature, is put to a TTL-NIM adapter and the output NIM signal is counted using a NIM scaler. The count rate of the detector in Hz is then calculated. Another output of the linear FIFO is fed to a Multi Channel Analyzer (MCA) to obtain the energy spectrum. A schematic representation of the set-up is shown in Figure 4.6.

Pre-mixed Ar/CO_2 in 70/30 and 90/10 volume ratios have been used for the whole study. A constant gas flow rate of 3.4 l/h is maintained using a Vögtlin gas flow meter.

For the measurements a circular patch of the detector is exposed with the X-ray from Fe^{55} source using two collimators of diameter 8 mm and 4 mm, corresponding to an area of $\sim$ 50 mm^2 and $\sim$ 13 mm^2 on the detector respectively.

4.4 Result

Ar/CO_2 in 70:30 ratio and a collimator made with G-10 material having diameter 8 mm has been used for this study. At first the bias voltage to the detector is increased and the count rate is measured

to get the exposure rate. It has been observed that as the efficiency of the detector increases with voltage so does the count rate and a plateau is observed from ΔV of 378.7 V onwards. ΔV across the top and bottom of GEM foil is same for all three GEM planes.

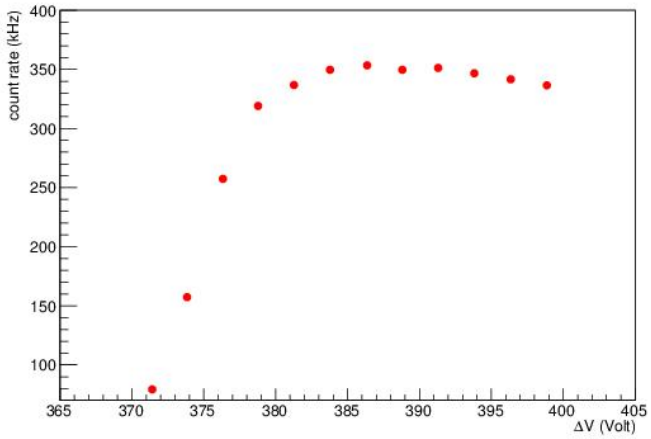

Figure 4.7: Count rate as a function of the GEM voltage.

The count rate as a function of bias voltage is shown in Figure 4.7. The saturated value of the count rate has been found to be $\sim$ 350 kHz which corresponds to a particle flux of 0.7 MHz/cm^2. This value of rate is used to calculate the accumulated charge later in this article. The gain and the energy resolution are measured from the energy spectrum for the Fe^{55} X-ray source. Figure 4.8 shows typical energy spectra recorded with Fe^{55} source at different ΔV.

The main peak (5.9 keV full energy peak) and the escape peak are clearly visible for all the voltage settings. The gain of the detector has been calculated by measuring the mean position of 5.9 keV peak of Fe^{55} X-ray spectrum with Gaussian fitting. The expression for the gain is given by [7],

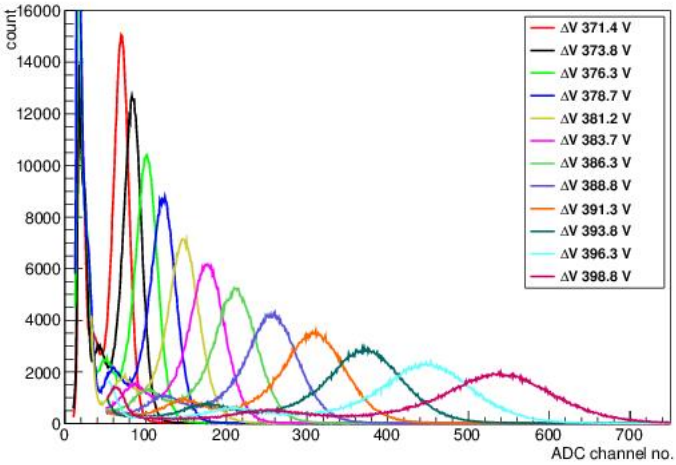

Figure 4.8: Energy spectra of the GEM detector at different GEM voltage

$$gain = \frac{output\ charge}{input\ charge} = \frac{(mean\ pulse\ height/2mV)fC}{number\ of\ primary\ electrons \times e\ C} \tag{4.1}$$

where the mean pulse height for 5.9 keV peak in ADC channel number is obtained by Gaussian fitting and that in mV is obtained from the ADC calibration curve (ADC channel no. vs pulse height). The preamplifier used in the set-up offers a gain of 2 mV/fC which has been used in the expression for gain. The input charge is the primary number of electrons produced in the gas detector as a result of total absorption of an X-ray photon of energy 5.9 keV, multiplied by the electronic charge (e). For each 5.9 keV Fe^{55} X-ray photon exposed in Ar/CO_2 gas with 70/30 ratio, the number of primary electrons approximately produced are 212.

The energy resolution of the detector is defined as[9],

$$energy\ resolution(\%) = \frac{sigma \times 2.355}{mean} \times 100 \tag{4.2}$$

where the sigma and the mean are obtained from the Gaussian fitting of the spectrum. It is understood that a lower value of energy resolution means a better energy resolution. The gain and energy resolution have been measured, increasing the biasing voltage of the detector.

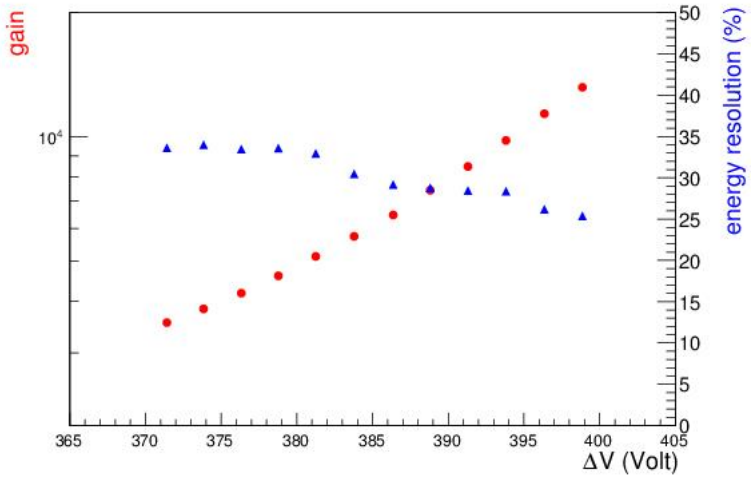

Figure 4.9: The gain and the energy resolution as a function of the GEM voltage.

Both the gain and the energy resolution as a function of ΔV across a GEM foil is shown in Figure 4.9.

It is observed that the gain increases exponentially from a value of $\sim$ 3500 to 14000 whereas the energy resolution value decreases from 34% to 25% (FWHM) with increasing voltage.

Same kind of measurements have been carried out using Ar/CO_2 in 90:10 ratio and using a perspex collimator having diameter 4 mm. Results are discussed below.

Since a perspex collimator having diameter 4 mm has been used, the rate is found to be $\sim$ 220 kHz which corresponds to a particle

flux of 1.7 MHz/cm^2. The number of primary electrons approximately produced are 223. A plateau is observed from ΔV $\sim$ 337 V on-wards as shown in the Figure 4.10.

It is observed that the gain increases exponentially from a value of $\sim$ 3000 to 10000 whereas the energy resolution value decreases from about 31% to 28% (FWHM) with increasing voltage as shown in the Figure 4.11, and also the energy spectrum for different GEM voltages is shown in the FIgure 4.11.

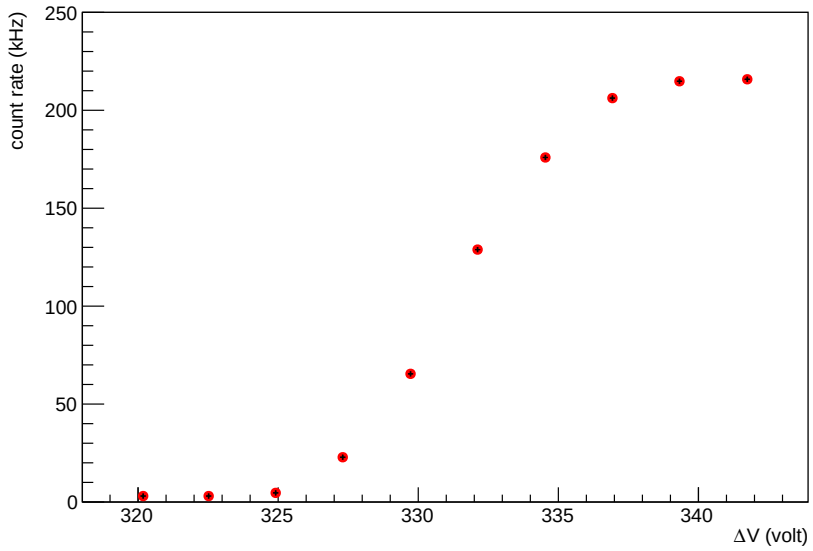

Figure 4.10: Count rate as a function of the GEM voltage

+

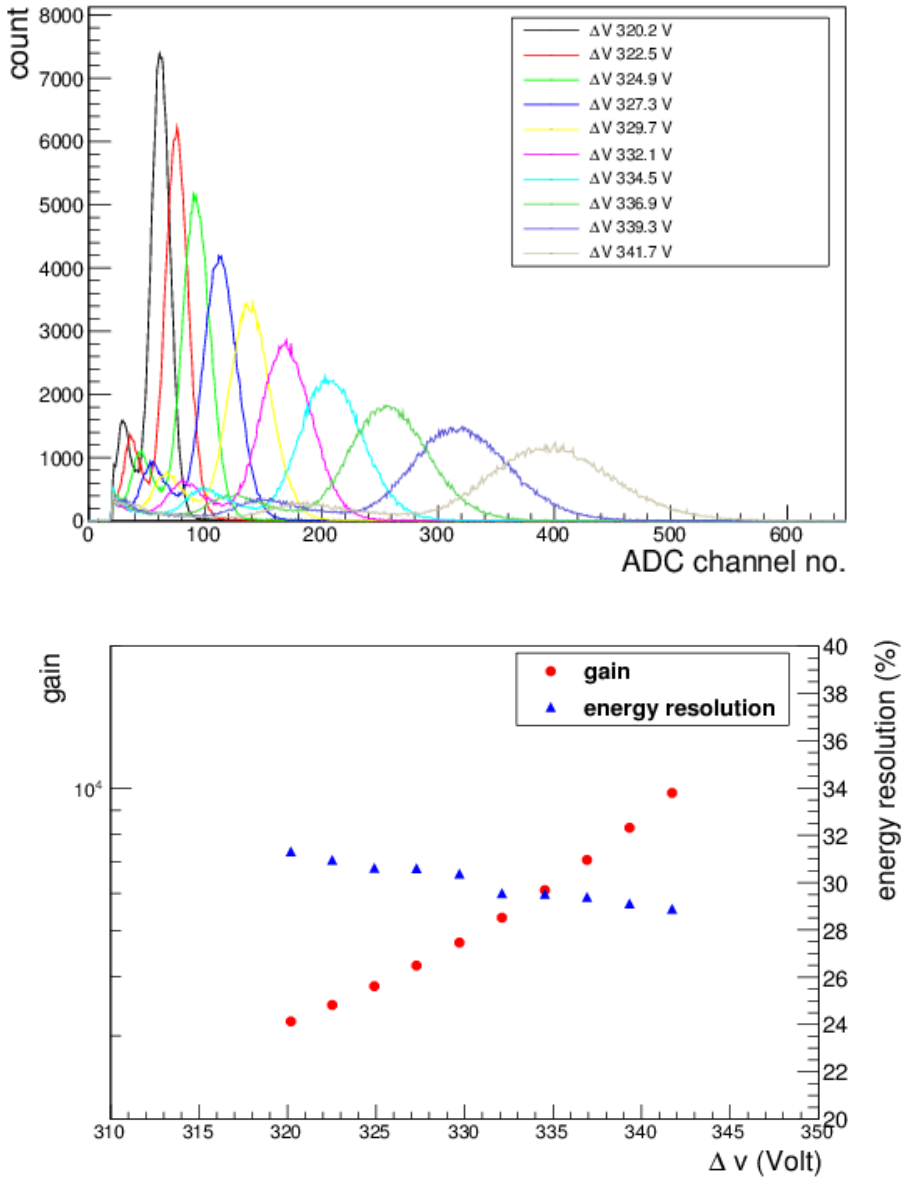

Figure 4.11: Energy spectra of the GEM detector at different GEM voltage (up) and the gain and the energy resolution as a function of the GEM voltage (down).

Chapter 5

Uniformity Study

5.1 Results of the Uniformity Study

To study the uniformity of gain, energy resolution, and particle count rate over the GEM detector central active region, premixed Ar/Co_2 in 70/30 ratio have been used. Gas flow rate has been kept constant at a rate of 3.4 litre/hour using gas flow meter. A 8 mm diameter collimator, which is made of G-10 material has been used to irradiate the detector with the X-ray from Fe^{55} source.

The gain, energy resolution are measured from the energy spectrum of the Fe^{55} X-ray source. After the voltage scan as described in the previous chapter, we observed a plateau in the count rate, which indicates the highest efficiency of the detector.

From that particular plot of count rate vs voltage as shown in the Figure 4.7, we have decided to apply -4100 volt to the detector as a biasing voltage and this corresponds to a $\Delta V \sim 384$ volt across each GEM foils.

The active area of the chamber (detector) has been divided into 100 zones of 1 cm^2, but since the readout pad is only in the central region, that is why the study of uniformity in terms of gain, energy resolution and particle count rate has been carried over a 5×4 array in the central region. Figure 5.1, 5.2, 5.3 respectively shows the uniformity in gain, energy resolution and particle count rate.

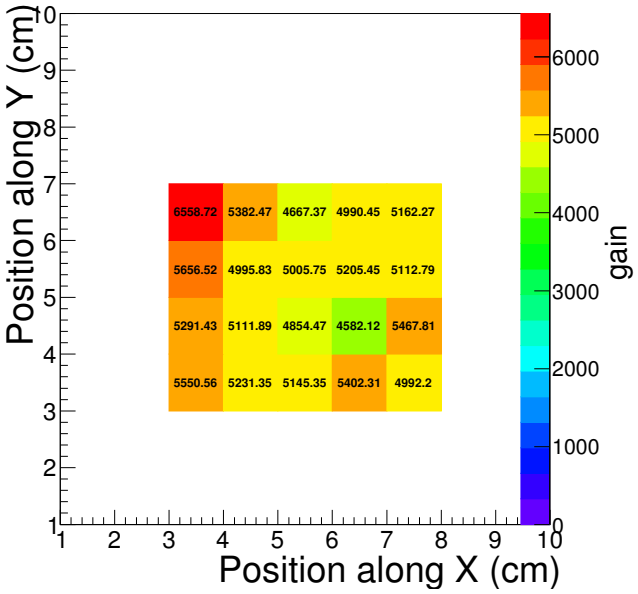

Figure 5.1: Uniformity in gain over the central active area of the detector

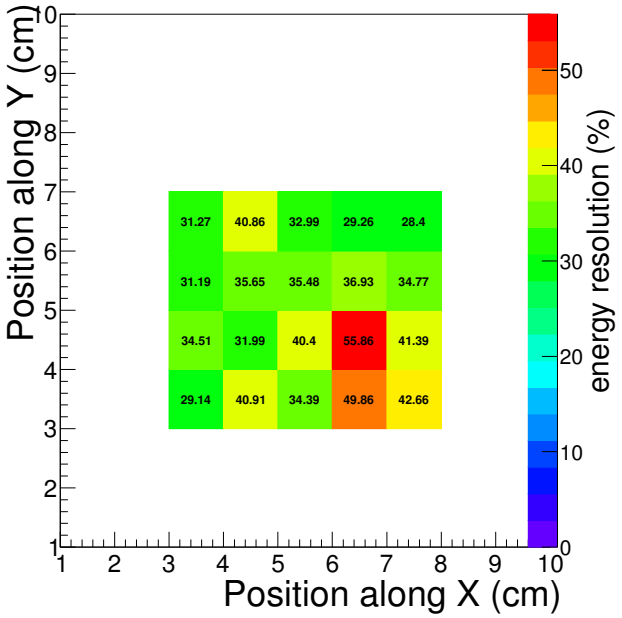

Figure 5.2: Uniformity in energy resolution over the central active area of the detector

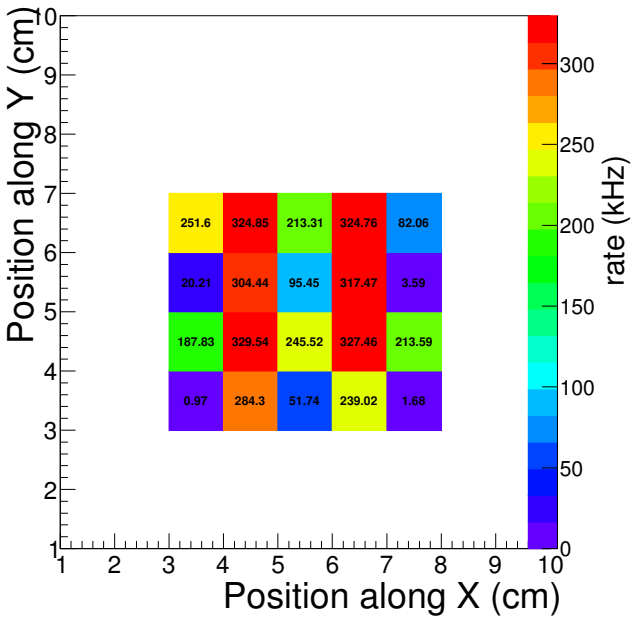

Figure 5.3: Uniformity in count rate over the central active area of the detector

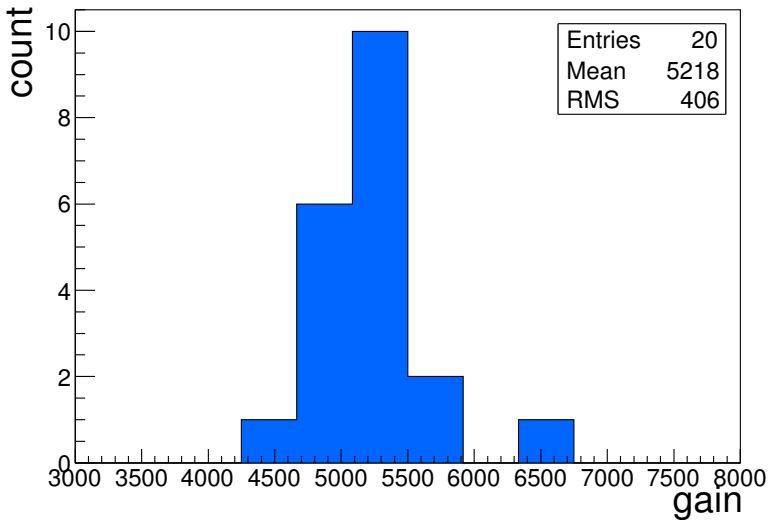

Figure 5.4: Distribution of gain over the active region of the detector

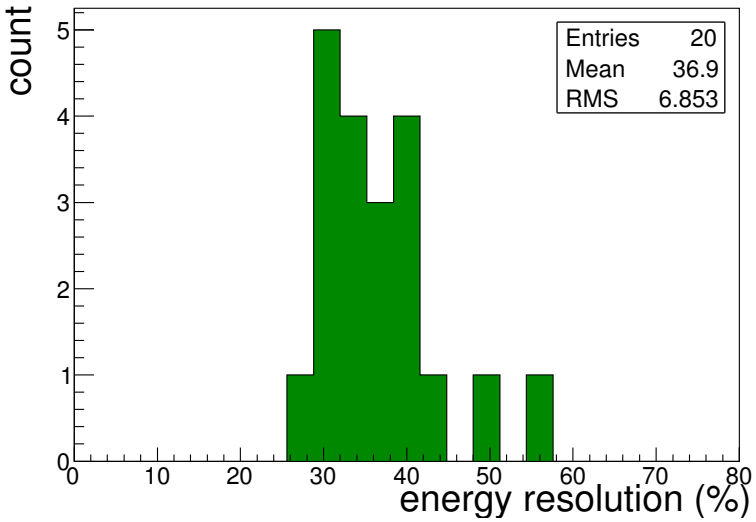

Figure 5.5: Distribution of energy resolution over the active region of the detector

Figure 5.4, 5.5, 5.6 respectively shows the variations of gain, energy resolution, count rate. For some zones the count rate has been found to be as low as 100 kHz. So for the distribution of the count rate a lower cut of 150 kHz has been used.

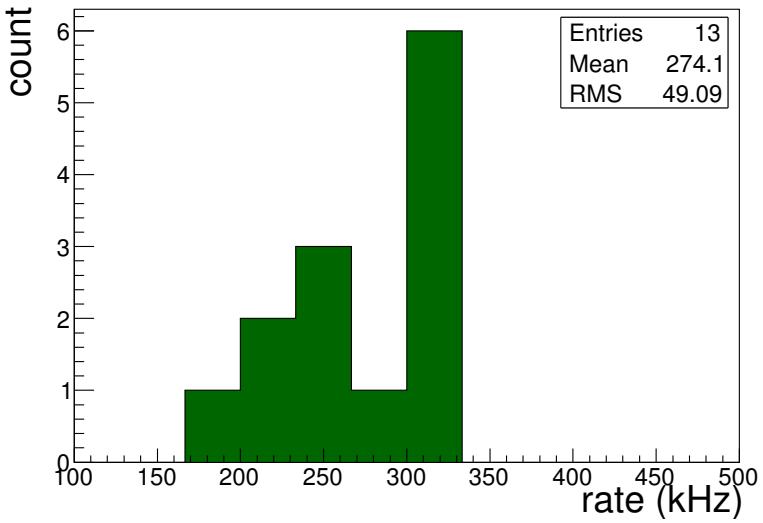

Figure 5.6: Distribution of count rate over the active region of the detector

5.2 Discussions

Due to the intrinsic inhomogeneity in the GEM foils and improper geometry and also for the inhomogeneity in the gap between GEM foils , a gain variation upto few percentage is possible. In this study the gain, energy resolution and count rate have been measured at 20 zones in the central active area of the triple GEM detector prototype using a Fe^{55} X-ray source. For each measurement an area of $\sim$ 50 mm^2 in the central part of each zones has been exposed by 5.9 KeV X-ray and the temperature, pressure are kept almost constant during the measurements. Over the measured area fluctuation in gain is found to be around 10% and the fluctuation in the energy resolution and count rate is found to be around 20% for Ar/CO_2 in the 70/30 ratio.

Chapter 6

Study of Stability

6.1 Results of the stability study

The same detector prototype has been used to study the long term stability of the detector. Using different collimators and gas mixtures, the variation in the gain and energy resolution with the temperature and pressure has been studied [8].

The stability test of the has been carried out with Ar/CO_2 gas mixture in 70/30 ratio at a HV of - 4100 V. The average current through the divider chain has been found to be ~ 699 μA producing a $\Delta V \sim 384$ V. With a collimator made of G-10, a circular area of ~ 50 mm^2 of the GEM detector is exposed from top with X-ray of rate ~ 350 kHz from a Fe^{55} source which is equivalent to a particle flux of 0.7 MHz/cm^2. The same source is used to irradiate the detector as well as to obtain the spectrum. The spectra are stored automatically using the ORTEC MCA at an interval of 10 minute. Since the gain of gaseous detector depends significantly on the ratio of temperature and pressure (T/p), according to the equation 6.1.

$$G(T/p) = Ae^{(B\frac{T}{p})} \tag{6.1}$$

the temperature (t in $^\circ C$) and pressure (p in mbar) are also recorded simultaneously using a data logger. CuteCom software package is used for automatic and continuous monitoring of the temperature and pressure. After setting up all things and applying $\Delta V = 384$ V the detector is kept for few hours for conditioning. The measure-

ment of gain and energy resolution is continued uninterruptedly for a period of > 1200 hours after the conditioning.

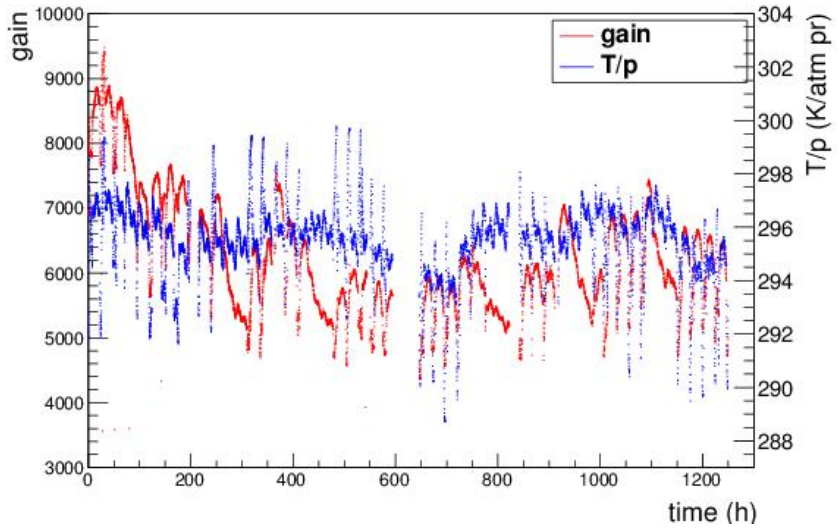

Figure 6.1: Variation of the measured gain and T/p as a function of the time.

The variation of the measured gain and T/p are plotted as a function of time in Figure 6.1, where T (= t+273) is the absolute temperature in Kelvin and p (p in mbar/1013) is in the unit of atmospheric pressure.

The gain vs. T/p correlation plot is drawn and fitted with the function given by equation 6.1 as shown in Figure 6.2 (the parameters A and B are marked as p0 and p1 respectively). After fitting the correlation plot the values of the fit parameters A and B obtained, are $0.005 \pm 4.11 \times 10^{-5}$ and $0.047 \pm 2.31 \times 10^{-5}$ atm/K respectively. The measured gain is normalised with the gain calculated from the equation 6.1.

To study the stability of the detector gain, the normalised gain is plotted as a function of the total charge accumulated per unit irradiated area of the GEM chamber, which is directly proportional to time. The charge accumulated at a particular time is calculated

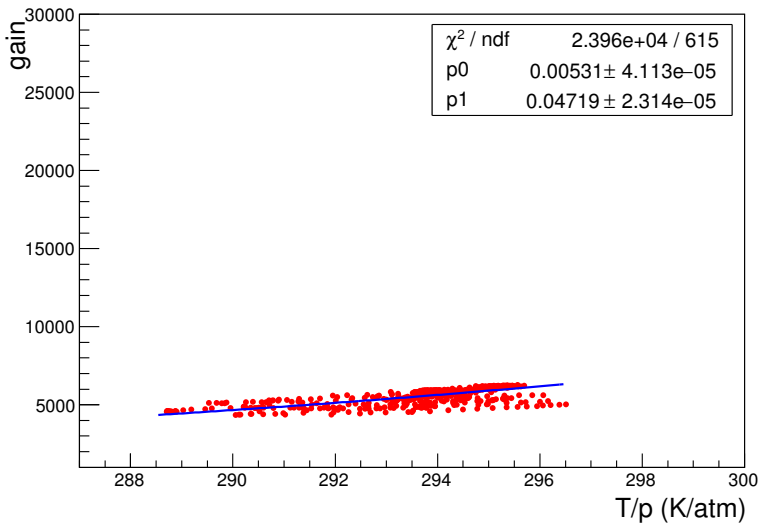

Figure 6.2: Correlation plot: Variation of the gain as a function of T/p.

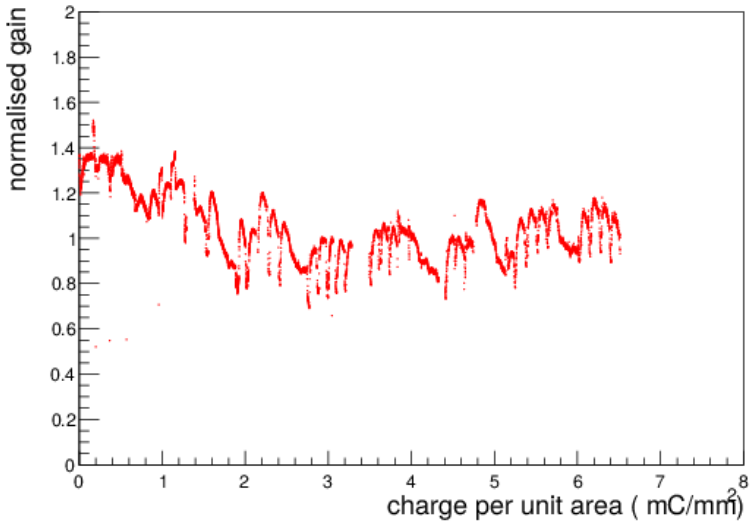

Figure 6.3: Variation of the normalised gain as a function of the charge per unit area i.e. dq/dA.

by

$$\frac{dq}{dA} = \frac{r \times n \times e \times G \times dt}{dA} \tag{6.2}$$

where, r is the measured rate in Hz incident on a particular area of the detector, dt is the time in second, n is the number of primary electrons for a single X-ray photon, e is the electronic charge, G is the gain and dA is the irradiated area. For each data point the charge is calculated in a time interval (10 minutes here) and it is summed up to get the total accumulated charge. In this test a total accumulation of charge per unit area $\sim$ 6.5 mC/mm^2 is achieved. The normalised gain as a function of the total accumulated charge per unit area is shown in Figure 6.3. The distribution of the normalised gain is shown in Figure 6.4.. The mean of the distribution has been found to be 1.054 with a rms of 0.15.

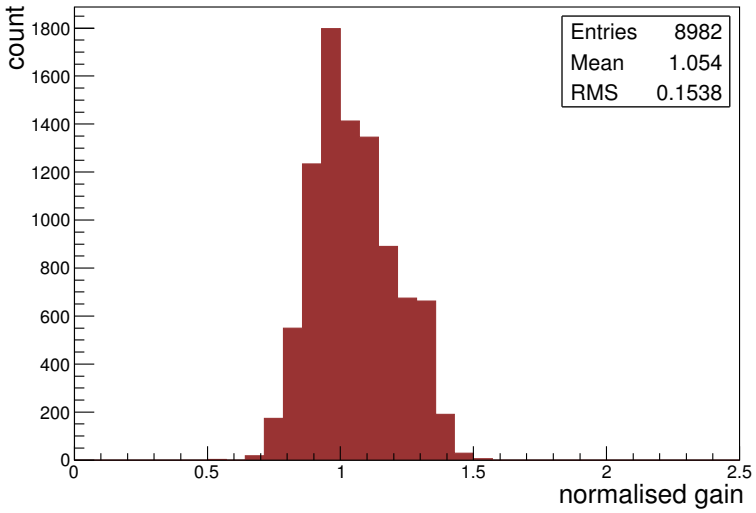

Figure 6.4: The distribution of the normalised gain.

One of the main goals of this study is also to measure the energy resolution continuously at high rate of radiation. The energy resolution as a function of the time is shown in Figure 6.5. The energy resolution in the whole period of measurement varied between 25% to 45% FWHM. The energy resolution is plotted as a function of

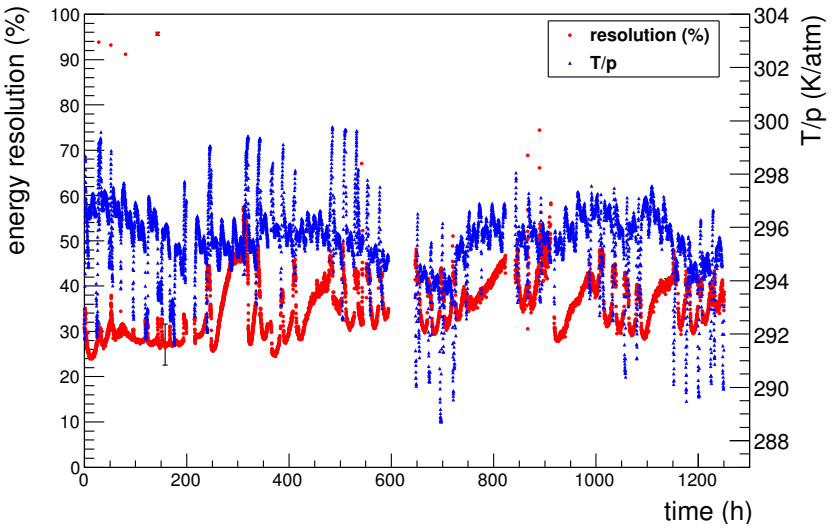

Figure 6.5: Variation of the energy resolution and T/p as a function of time.

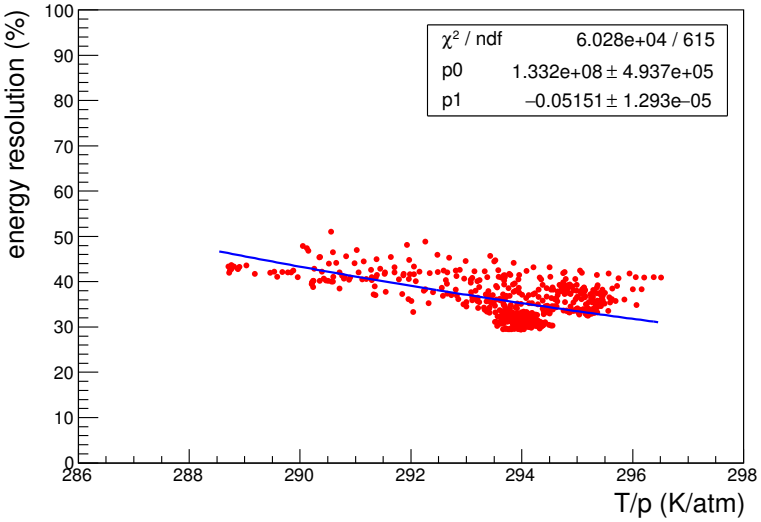

Figure 6.6: Energy resolution as a function of T/p.

T/p and is shown in Figure 6.6. The energy resolution improves

with increase of T/p. In the present study, the correlation curve is fitted with an exponential function:

$$energy\ resolution = A' e^{(B' \frac{T}{p})} \tag{6.3}$$

where A' and B' are the fit parameters (in Figure 6.6 the parameters A' and B' are marked as p0 and p1 respectively). The value of A' and B' obtained from the fitting are $1.33 \times 10^8 \pm 4.93 \times 10^5$ and -0.05 $\pm$ 1.29 $\times$ 10^{-5} atm/K. The measured energy resolution is normalised with the energy resolution value calculated from the equation 6.3.

The normalised energy resolution is plotted as a function of the total accumulated charge per unit area and shown in Figure 6.7 .

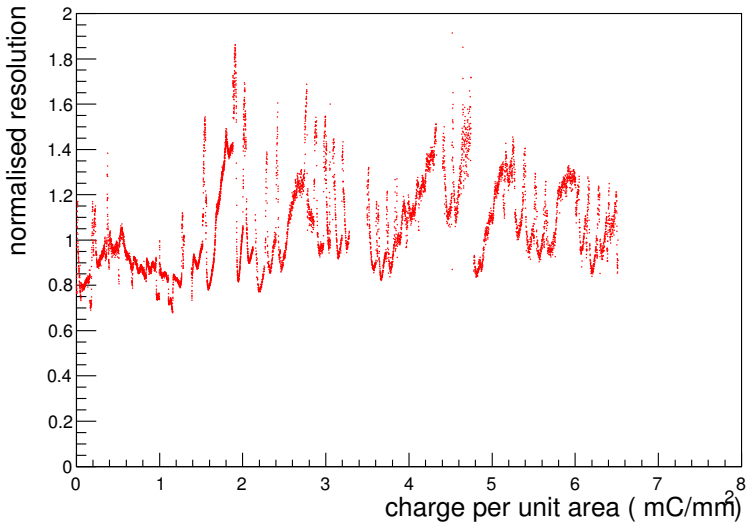

Figure 6.7: Normalised energy resolution as a function of the charge per unit area.

The distribution of the normalised energy resolution is shown in Figure 6.8. The distribution shows that after a period of $>$ 1200

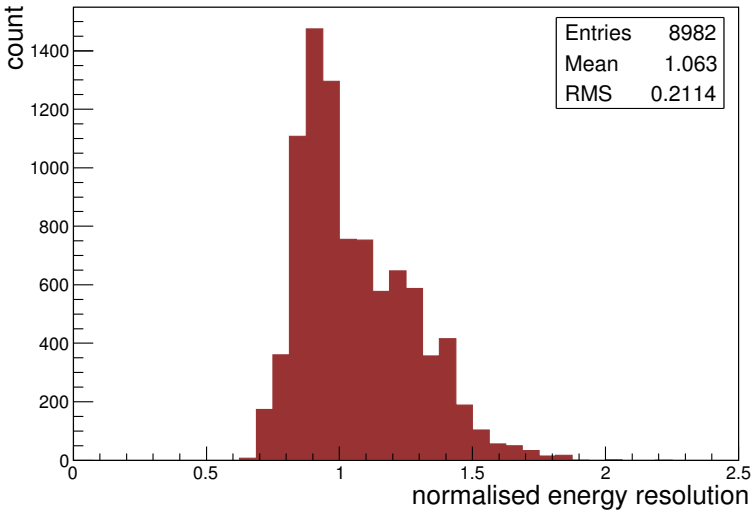

Figure 6.8: The distribution of the normalised energy resolution.

hours of continuous radiation, the mean normalised energy resolution is 1.063 with a rms of 0.21.

The same measurement has been done with Ar/CO_2 gas mixture in 90/10 ratio and with a Perspex collimator having diameter 4 mm. Particle flux is about 1.7 MHz/cm^2. It has been carried out at a HV -3625 V. The average current through the divider chain has been found to be $\sim$ 604 μA producing a ΔV $\sim$ 332 V. The measurement of gain and energy resolution is continued uninterruptedly for a period of $>$ 300 hours. The results are discussed below.

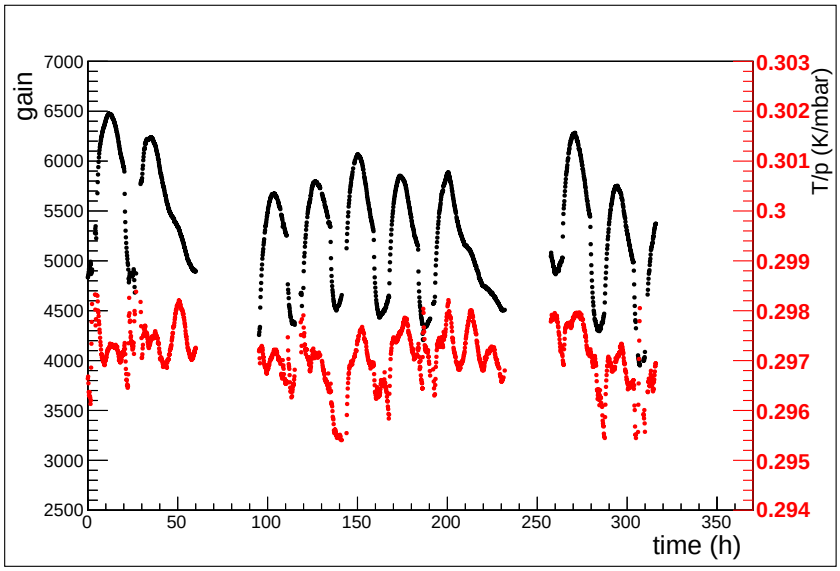

Figure 6.9: Variation of the measured gain and T/p as a function of the time

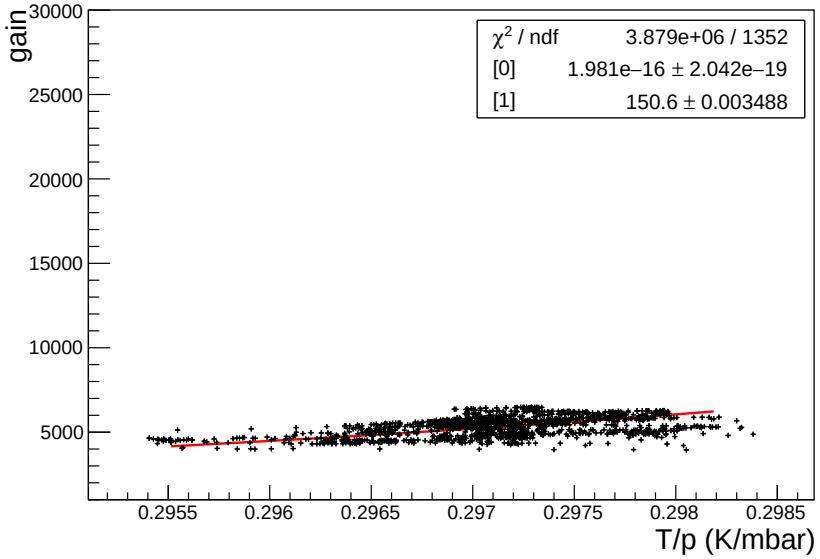

Figure 6.10: Correlation plot: Variation of the gain as a function of T/p

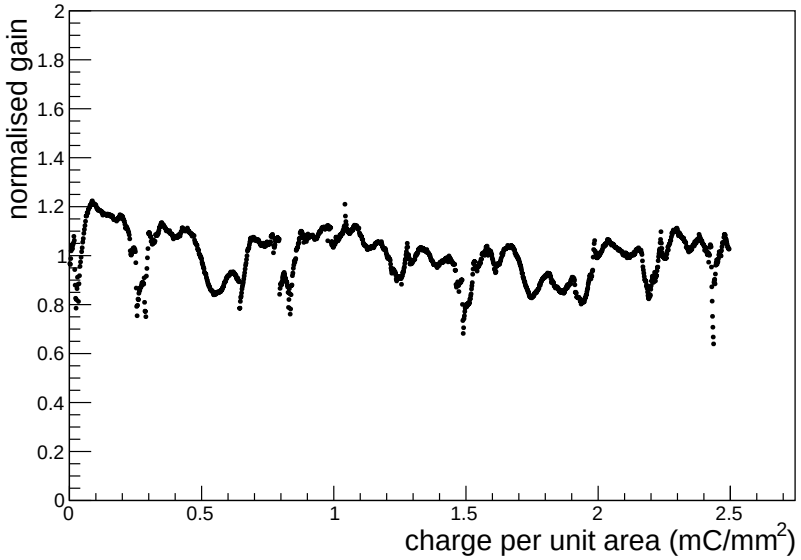

Figure 6.11: Variation of the normalised gain as a function of the charge per unit area

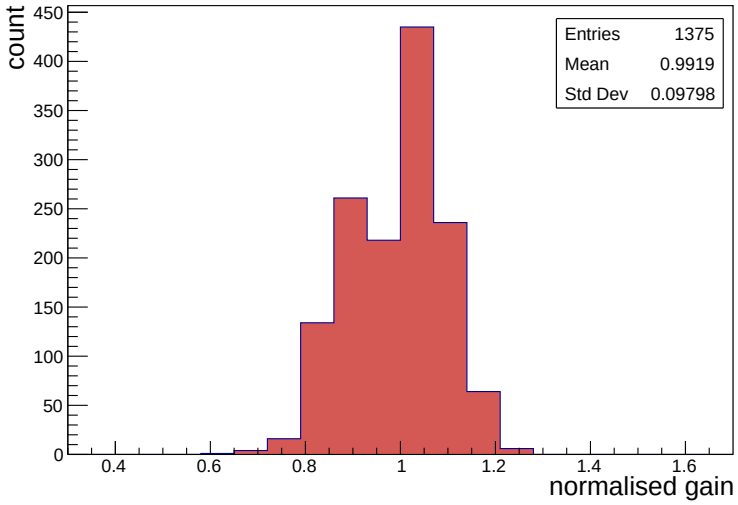

Figure 6.12: Distribution of normalised gain

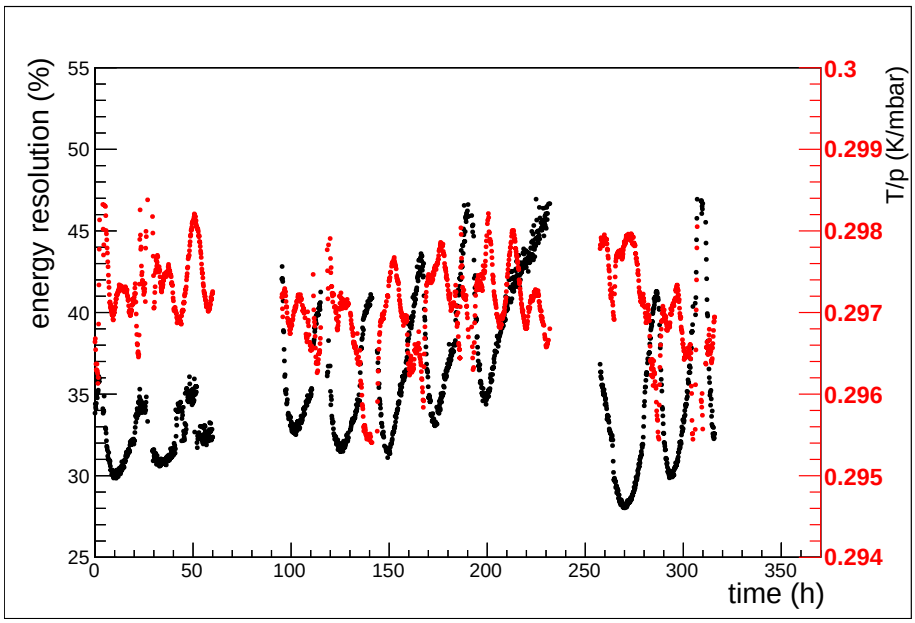

Figure 6.13: Variation of the energy resolution and T/p as a function of time

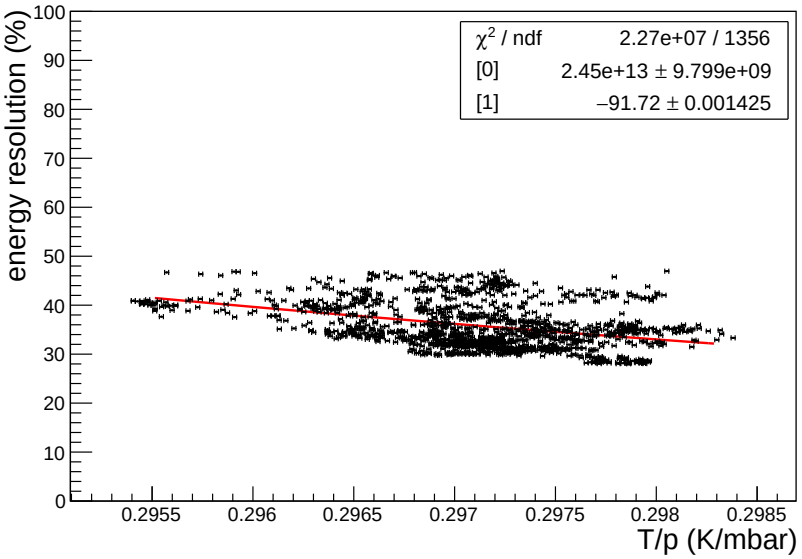

Figure 6.14: Correlation plot: Energy resolution as a function of T/p

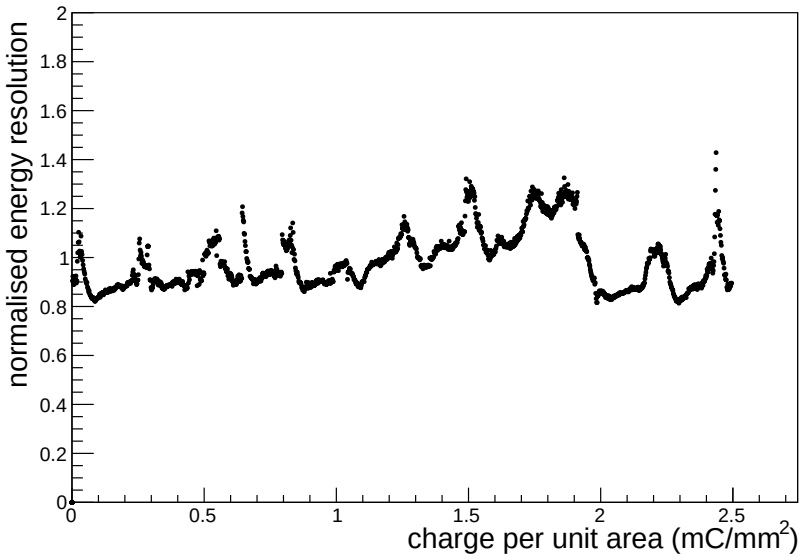

Figure 6.15: Normalised energy resolution as a function of charge per unit area

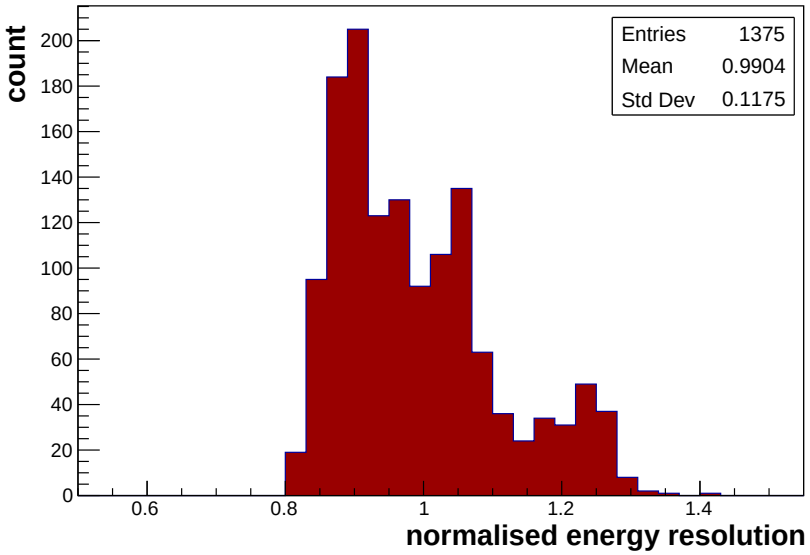

Figure 6.16: Distribution of the normalised energy resolution

6.2 Discussions

A systematic study on stability of the gain and energy resolution of a triple GEM detector in long term operation under high rate of X-ray irradiation is performed with Ar/CO_2 gas mixture in 70/30 and 90/10 ratios, using the conventional NIM electronics. In this study the same Fe^{55} source is used to irradiate the chamber as well as to measure the gain and energy resolution at an interval of 10 minutes. Using a collimator the rate of the incident X-ray has been fixed to $\sim$ 350 kHz on an area of $\sim$ 50 mm^2 of the GEM detector with 70/30 gas mixture and $\sim$ 220 kHz on an area of $\sim$ 13 mm^2 with 90/10 gas mixture. In this study for the first time the detector has been continuously exposed to high rate of X-ray radiation for $>$ 1200 hours with Ar/CO_2 in 70/30 ratio and then for $>$ 300 hours with 90/10 gas mixture. To collect the signals from the detector a charge sensitive preamplifier (VV50-2) is used with gain 2 mV/fC and shaping time 300 ns. In a continuous operation of $>$ 1200 hours or an equivalent accumulated charge per unit area of $\sim$ 6.5 mC/mm^2 the mean normalised gain and the mean normalised energy resolution have been found to be 1.054 with a rms of 0.15 and 1.063 with a rms of 0.21 respectively, and for the continuous operation with 90/10 mixture results in accumulation of charge per unit area about 2.5 mC/mm^2 with mean normalised gain about 0.9919 with a rms 0.098 and mean normalised energy resolution about 0.9904 with rms 0.1175. The prototype under test did not show any significant degradation even after the exposure of the radiation over the long time.

Chapter 7

Summary and Future Plans

7.1 Summary

A study of basic characteristics of the triple GEM detector have been carried out with premixed gas of Ar/CO_2 in 70/30 and 90/10 ratios using conventional NIM electronics. In this study count rate, effective gain, energy resolution are measured with a strong Fe^{55} X-ray source using two different collimator having different dimensions. The gain and energy resolution are measured from the Fe^{55} spectra varying the voltage. The gain increases exponentially and energy resolution decreases with voltage.

Uniformity in gain, energy resolution, count rate over the central active region of the detector has been investigated with Ar/CO_2 in 70/30 ratio using a G-10 collimator having dimension 8 mm. We obtained around 10% fluctuation in the gain and around 20% fluctuation in the energy resolution and in the count rate over the central region of the chamber. Due to the intrinsic inhomogeneity in the GEM foils and improper geometry and also for the inhomogeneity in the gap between GEM foils, a gain variation upto few percentage is possible.

A systematic study on stability of the gain and energy resolution of a triple GEM detector in long term operation under high rate of X-ray irradiation is performed with Ar/CO_2 gas mixture in 70/30 & 90/10 ratios and using different collimators. G-10 collimator (hav-

ing diameter 8 mm) has been used for the 70/30 gas mixture and Perspex collimator (having diameter 4 mm) for the 90/10 mixture. In this study the same Fe^{55} source is used to irradiate the chamber as well as to measure the gain and energy resolution at an interval of 10 minutes.

In a continuous operation of >1200 hours under high rate of X-ray radiation with 70/30 gas mixture and after an equivalent accumulated charge per unit area of 6.5 mC/mm^2 the mean normalised gain and the mean normalised energy resolution have been found to be 1.054 with a rms of 0.15 and 1.063 with a rms of 0.21 respectively. The continuous operation with 90/10 mixture results in accumulation of charge per unit area about 2.5 mC/mm^2 with mean normalised gain about 0.9919 with a rms 0.098 and mean normalised energy resolution about 0.9904 with rms 0.1175. The prototype under test did not show any significant degradation in its performance.

7.2 Future Plans

Since our main goal is the CBM experiment, so we have to built a large GEM detector, which will be used in the real experiment, and also have to perform all the measurements I have done in this project. Our immediate goal is to develop a segmented readout so that we can measure the position resolution of the detector prototype. Also the efficiency measurement of the chamber is in future plans.

Bibliography

[1] Simulation, Design and Construction of a Gas Electron Multiplier for Particle Tracking by Andrej Sipaj. http://hdl.handle.net/10155/293

[2] https://fair-center.eu/for-users/experiments/cbm-and-hades/cbm.html

[3] Radiation detection and measurment by Glenn F. Knoll.

[4] Techniques for nuclear and particle physics experiments by William R. Leo.

[5] Characterisation of scintillator and gaseous detectors, and Measurement of angular variation of cosmic ray flux with scintillator detector by Shreya Roy

[6] Fabio Sauli. Operating principles and applications. Nuclear Instruments and Methods in Physics Research Section A: Accelerators, Spectrometers, Detectors and Associated Equipment, 805:2 24, 2016.

[7] S. Roy et al. Studies of the effect of rate on gain for straw tube detector. arXiv:1709.08030v1

[8] R.P. Adak et al. Long-term stability test of a triple gem detector. Journal of Instrumentation, 11(10):T10001, 2016.

[9] S. Roy et al. Study of stability of gain and energy resolution for GEM detector in high rate operation. arXiv:1804.02819

Outcomes

- **Study of uniformity of characteristics over the surface for triple GEM detector**

  Authors: **S. Chatterjee**, S. Chakraborty, S.Roy, S. Biswas, S. Das, S. K. Ghosh, S. K. Prasad, S. Raha

  Presented in **14th Pisa Meeting on Advanced Detectors, La Biodola, Isola d'Elba (Italy), submitted in NIM-A**

- **Stability study of gain and energy resolution for GEM detector**

  Authors: S. Roy, S. Rudra, S.Shaw, S. Chakraborty, **S. Chatterjee**, R. P. Adak, S. Biswas, S. Das, S. K. Ghosh, S. K. Prasad, S. Raha

  Presented in **14th Pisa Meeting on Advanced Detectors, La Biodola, Isola d'Elba (Italy), submitted in NIM-A**

- **A new type of RPC with very low resistive plates**

  Authors: S. Chakraborty, **S. Chatterjee** , S.Roy, A.Roy, S. Biswas, S. Das, S. K. Ghosh, S. K. Prasad, S. Raha

  Presented in **14th Pisa Meeting on Advanced Detectors, La Biodola, Isola d'Elba (Italy), submitted in NIM-A**